This is a previous version of the article published in Fluid Phase Equilibria. 2021, 546: 113124. https://doi.org/10.1016/j.fluid.2021.113124

An equation of state based on the intermolecular potential and the radial distribution function to estimate the virial coefficients by using PvT chaotic data

Manuel Pérez-Molina[a,b] Manuel F. Pérez-Polo[a,b*], Javier Gil Chica[a,b], Elena Fernández Varó[c,b]

[a]Departamento de Física, Ingeniería de Sistemas y Teoría de la Señal, Escuela Politécnica Superior, Universidad de Alicante.[b]Instituto de Física Aplicada a las Ciencias y las Tecnologías. Universidad de Alicante. [c]Departamento de Óptica, Farmacología y Anatomía. Universidad de Alicante.[a,b,c]E-mails: manuelpm@ua.es, manolo@dfists.ua.es, gil@dfists.ua.es, elena.fernandez@ua.es

Abstract

We derive a new equation of state (EOS) for any non-polar, polar or quantum gas and any intermolecular potential through an approximation of the radial distribution function based on the Ornstein-Zernike equation. Such EOS is applied to estimate the virial coefficients B and C using two approaches. On one hand, B and C are directly computed from the proposed EOS considering the Mie potential for neon and water steam, which leads to values in very good agreement with the experimental data. On the other hand, the proposed EOS is applied in the context of a thermodynamic model to estimate B and C by fitting the simulated chaotic PvT data at an almost constant temperature. Such estimations of B and C are compared with the experimental values, which allows elucidating if B and C have a significant contribution on the virial equation at the considered pressures and temperatures. This methodology is applied to nitrogen and helium4 considering the intermolecular potentials of Mie, Morse, Kihara and Buckingham. For the considered gases and intermolecular potentials, the calculated values of B and C are in very good agreement with experimental data in a wide range of pressures and temperatures.

Keywords: Radial distribution function, intermolecular potentials, thermodynamic model, chaotic behavior, equation of state, virial coefficients

* Author to whom correspondence should be addressed.

1 Introduction

The interacting theory of real gases based on an intermolecular potential with a hard core and a weak attractive region is widely recognized as one of the great successes of Statistical Mechanics. Two examples of such intermolecular potentials are the Mie *(n,m)* potential and the Lennard-Jones (12.6) potential (LJ), which can be considered as a particular case of the Mie potential [1,2]. These potentials have been used to determine thermodynamic quantities of real gases, such as, the virial coefficients, internal energy, enthalpy, density, Helmholtz free energy and heat capacity [3,4].

Besides the LJ potential, the Stockmayer potential (ST) has been used for polar fluids [5,6] whereas the Morse potential (MO) was initially used to determine the oscillating states and energies of a quantum oscillator [7]. In fact, there is a close relationship between the LJ and MO potentials as shown in Ref [8]. On the other hand, the Kihara potential (KI) modifies the hard core of the LJ potential and can be applied to non-spherical molecules that can be treated as convex rigid bodies [8,9]. Nonetheless, the KI potential can also be used assuming that the molecules have a spherical nucleus (as it will be done in this paper) [10]. Another extension of the LJ potential is the Buckingham potential (BU or Exp-6), which has been used with non-polar gases but modifying the molecule hard core [10], [11].

In the study of intermolecular potentials, it is assumed that the potential energy is a pairwise sum, i.e., the potential is equal to the sum of the pair of molecule potentials $V(r_{ij})$, being r_{ij} the distance between molecules i and j [2], [12]. The radial (or pair) distribution function (RDF) $g(r,\rho,T)$ is obtained by dividing the local densities $\rho(r)$ at various distances r of the molecule j by the bulk average density ρ at a given temperature T. The experimental determination of $g(r,\rho,T)$ is rather cumbersome and has been achieved from X-ray and neutron scattering experiments [13]. The pairwise sum assumption together with the knowledge of $g(r,\rho,T)$ allows to establish the equations for the pressure and internal energy, from which all the thermodynamic properties of a given gas can be deduced [14,15].

In this paper we derive theoretically an approximate RDF to obtain a general equation of state (EOS) that can be used with any real gas and intermolecular potential.

Such general EOS is applied to estimate the virial coefficients B and C using two approaches. On one hand, B and C are directly computed from the proposed EOS for neon and water steam considering the Mie potential, which leads to results in very good agreement with the experimental data. On the other hand, we consider a thermodynamic model aimed to achieve a chaotic gas dynamic to estimate B and C [16], which will be applied to nitrogen and helium4 using the Mie, Morse, Kihara and Buckingham potentials. The parameters of the thermodynamic model are defined in agreement with well stablished commercial or industrial devices [17-19]. The values of B and C estimated from the model are compared with the experimental data, which allows elucidating if B and C have a significant contribution on the virial equation at the considered pressures and temperatures. The estimated values of B and C are in very good agreement with experimental data in wide ranges of pressures and temperatures.

The thermodynamic model considers a mechanical subsystem which includes an input valve [20-21], a flow controller and pressure probe as well as a thermal subsystem formed by another flow controller, a heating-cooling coil and an accumulator vessel. The gas flow rate in the input valve is assumed to be isentropic, whereas the density, the heat capacity at constant volume and the pressure are calculated from the internal energy equations and the proposed equation of state, which depend on $V(r_{ij})$ and the RDF [16], [22], [23].

For the calculation of the second virial coefficient B, the quantum corrections will be included for neon and helium4, whereas dipole-dipole and quadrupole-quadrupole interactions will be considered for water steam and nitrogen respectively [24,25]. In addition, the gas polarization will be included by considering an approximation of the Axilrod-Teller-Muto potential [26,27] (which accounts three-body interactions) in which the molecules are at the vertices of an equilateral triangle. Other treatments for the polarization can be found in Refs [2], [15] and [28-30], whereas the background of three-body interactions between dipoles and quadrupoles can be found in Refs [29], [30] and references contained therein.

The effect of the intermolecular potential in the calculation of C could be also analyzed from the perturbation theory by using a hard-sphere system as a reference system (unperturbed system) and an additional Lennard-Jones potential (perturbed

system) to obtain an equivalent potential formed by a hard-sphere potential with a temperature dependent diameter. For details see Ref [31] and the papers cited therein. In this paper we use an approximation of the radial distribution function based on the Ornstein-Zernike equation [32], which allows using the internal energy and pressure equations for the calculation of the third virial coefficient.

2 General equation of state relying on an approximate radial distribution function

Under the assumption of pairwise additivity for the intermolecular potential, the thermodynamic properties of a fluid can be determined according to [14], [15]:

$$\Delta U = 2\pi \frac{N_A}{M^2} \rho_m \int_0^\infty u\left(r,T\right) g\left(r,\rho,T\right) r^2 \mathrm{d}r \tag{1}$$

$$P = \frac{N_A}{M} kT\rho_m - \frac{2\pi}{3} \frac{N_A}{M^2} \rho_m^2 \int_0^\infty \left(r \frac{\partial u\left(r,T\right)}{\partial r} \right) g\left(r,\rho,T\right) r^2 \mathrm{d}r \tag{2}$$

where ΔU is the variation of the gas internal energy (J), N_A and k are the Avogadro number (mol^{-1}) and Boltzmann constant (in J/K) respectively, M is the molecular mass, $u(r,T)$ is the intermolecular potential (J), ρ_m is the gas mass density ($\mathrm{kg/m^3}$), P is the gas pressure ($\mathrm{N/m^2}$) and $g(r,\rho,T)$ is the RDF being $\rho = \rho_m N_A / M$ the gas density ($\mathrm{molecules/m^3}$). It should be noted that the intermolecular potential is independent of the temperature for non-polar gases and temperature dependent for polar gases (see Eqs (A10)-(A13) of the Appendix). Once the intermolecular potential and the RDF are established, Eq (2) becomes an equation of state (EOS) that can be used with any real gas and intermolecular potential.

In order to establish a RDF we start from the well-known cluster expansion method, according to which the values of $B(T)$ and $C(T)$ at each temperature T for a given intermolecular potential u_{ij} can be calculated according to [14],[15]:

$$B(T) = -2\pi N_A \int_{V_e} f_{ij} r_{ij}^2 \mathrm{d}r_{ij} \;\; ; \;\; f_{ij} = e^{-u_{ij}/kT} - 1 \tag{3}$$

$$C(T) = C_{123}(T) + C_M(T) \tag{4}$$

where f_{ij} is the Mayer function associated to the interaction of two molecules, whereas $C_{123}(T)$ and $C_M(T)$ are defined as:

$$\begin{aligned} C_{123}(T) &= -\frac{8\pi^2}{3} N_A^2 \int_{V_e} f_{12} f_{13} f_{23} \mathrm{d}r_{12} \mathrm{d}r_{13} \mathrm{d}r_{23} \;\; ; \; f_{ij} = e^{-u_{ij}(\vec{r},T)/kT} - 1 \\ C_M(T) &= -\frac{8\pi^2}{3} N_A^2 \int_{V_e} (1+f_{12})(1+f_{13})(1+f_{23}) f_M \mathrm{d}r_{12} \mathrm{d}r_{13} \mathrm{d}r_{23} \;\; ; \; f_M = e^{-u_M(\vec{r})/kT} - 1 \end{aligned} \tag{5}$$

In Eq (5), the terms $C_{123}(T)$ and $C_M(T)$ are respectively the contributions to the virial coefficient C due to three-molecule interaction and polarization of the molecules, being the latter described by the Axilrod-Teller-Muto potential u_M [26], [27], [28]:

$$u_M(\theta_{ijk}, r_{ij}) = \upsilon \frac{(1 + 3\cos\theta_i \cos\theta_j \cos\theta_k)}{(r_{ij} r_{ik} r_{jk})^3} \;\; ; \;\; \upsilon = \frac{9}{16} \alpha^3 I_0 \tag{6}$$

where α and I_0 are respectively the polarizability (m^3) and the first ionization potential (J), θ_i (θ_j and θ_k) is the angle subtended at molecule i (j and k) by the other two molecules, r_{ij}, r_{ik}, r_{jk} are the sides of the atomic triangle and υ is the non-additive coefficient. The latter is related to interactions between three dipoles, which can be either induced dipoles for non-polar gases or permanent dipoles for polar gases. According to Eq (6), the values for υ expressed in atomic units for argon, krypton and xenon are 457.77, 1439.7 and 6606.1 respectively, which are in agreement with the respective values 518.3, 1572 and 5573 used in Refs [29], [30]. In the case of neon, water steam, nitrogen and helium4 considered in this paper, the values of υ expressed in atomic units are 13.46, 461.46, 939.60 and 2.23 respectively.

By assuming that the three interacting molecules form an equilateral triangle, we consider an approximation of Eq (6) given by:

$$u_M(r) = \frac{f_{CM} I_0 \alpha^3 \left(1 + 3\cos^3 60^o\right)}{r^9} \tag{7}$$

where f_{CM} is a variable fitting factor that depends on the considered gas and intermolecular potential, and it will be positive to represent a repulsive interaction. For each gas and intermolecular potential, a first estimation of f_{CM} is obtained by imposing that $u_M(r = \sigma) = \varepsilon$ being ε and σ the Lennard-Jones potential parameters (see Eq (A2)), which leads to the estimate $(8/11)\varepsilon\sigma^9/(I_0\alpha^3)$. Such estimate provides the magnitude order for f_{CM}, which will then be fitted to reproduce the experimental values of virial coefficients B and C. In particular, the values of f_{CM} will imply that the polarization effects will be significant at low temperatures but will become negligible at high temperatures. For the gases Ne, H_2O, N_2 and He4 considered in this paper, the first estimates $(8/11)\varepsilon\sigma^9/(I_0\alpha^3)$ of f_{CM} are 19.32, 2.32, 8.84 and 15.82 respectively. The low value of 2.32 obtained for water steam is due to its high dipolar moment, and consequently $u_M(r = \sigma)$ will be greater than ε.

In the low-density limit, the RDF can be expressed as [14]:

$$g(r,0,T) = \lim_{\rho \to 0} g(r,\rho,T) = e^{-u(r,T)/kT} \tag{8}$$

According to Eq (8), the radial distribution function $g(r,\rho,T)$ can be expanded in power series of the density ρ as follows:

$$g(r,\rho,T) = e^{-u(r,T)/kT}\left[1 + \rho g_1(r,T) + \rho^2 g_2(r,T) + ...\right] \tag{9}$$

where the first term in the series considers interactions between two molecules and is used to obtain the virial coefficient B, the second term considers interactions between three molecules and provides the virial coefficient C, and so on. Substituting Eq (9) into Eq (2) it is possible to express the equation of state as:

$$\frac{PM}{N_A kT\rho_m} = 1 - \frac{2\pi}{3}\frac{N_A}{MkT}\rho_m \int_0^\infty \left(r\frac{\partial u(r,T)}{\partial r} \right) e^{-u(r,T)/kT} r^2 \mathrm{d}r - \\ -\frac{2\pi}{3}\frac{N_A}{MkT}\rho_m^2 \int_0^\infty \left(r\frac{\partial u(r,T)}{\partial r} \right) e^{-u(r,T)/kT} g_1(r,T) r^2 \mathrm{d}r - \ldots\ldots \tag{10}$$

where only the function $g_1(r,T)$ (which considers interactions between three molecules) is considered, since for real gases there are no experimental data for the virial coefficients D, E and so on. From Eq (10) it is possible to derive the expressions for the virial coefficients B and C taking into account that B only depends on the intermolecular potential whereas C also depends on the function $g_1(r,T)$ at each temperature T. The general expression for $g_1(r,T)$ is given by [14], [31], [32]:

$$g_1(\vec{r}_{12},T) = \int_V \left[e^{-u(\vec{r}_{13})/kT} - 1 \right] \left[e^{-u(\vec{r}_{23})/kT} - 1 \right] \mathrm{d}\vec{r}_3 \tag{11}$$

where r_{ij} are the distances between molecules i and j, the integration must be done for all possible values of molecule 3 position and the integration volume V extends to infinity given that the intermolecular potentials decrease very rapidly.

To simplify Eq (11) to a scalar equation that can be more easily used from a computational viewpoint by substituting it in Eq (2), we will deduce an approximation based on the Ornstein-Zernike equation, which has been widely used in the theory of dense fluids [15]. Such equation is formed by a series of non-linear integral equations which consider that the total correlation function $h(\vec{r}_{12})$ between two molecules is the sum of a direct effect named the direct correlation function $c(\vec{r}_{12})$ plus an indirect effect due to the rest of molecules, i.e.:

$$h(\vec{r}_{12}) = c(\vec{r}_{12}) + \rho \int c(\vec{r}_{13}) h(\vec{r}_{23}) \mathrm{d}\vec{r}_3 \\ h(\vec{r}_{12}) = g(\vec{r}_{12}) - 1 = e^{\frac{-u(\vec{r}_{12},T)}{kT}} - 1 \tag{12}$$

where ρ is the number of molecules per unit of volume and $h(\vec{r}_{12})$ coincides with the Mayer function for the two molecules 1 and 2. By expanding Eq (12) to take into account the effects of the molecules 3, 4 and so on, it is obtained that:

$$\begin{aligned} h(\vec{r}_{12}) &= c(\vec{r}_{12}) + \rho \int c(\vec{r}_{13}) h(\vec{r}_{23})\, \mathrm{d}\vec{r}_3 \\ h(\vec{r}_{23}) &= c(\vec{r}_{23}) + \rho \int c(\vec{r}_{24}) h(\vec{r}_{34})\, \mathrm{d}\vec{r}_4 \\ h(\vec{r}_{34}) &= c(\vec{r}_{34}) + \rho \int c(\vec{r}_{34}) h(\vec{r}_{45})\, \mathrm{d}\vec{r}_5 \\ &\ldots\ldots\ldots\ldots\ldots\ldots\ldots\ldots\ldots\ldots\ldots\ldots \end{aligned} \tag{13}$$

In Eq (13), by substituting into the expression of $h(\vec{r}_{12})$ the expressions of $h(\vec{r}_{23}), h(\vec{r}_{34})$ and so on it follows that:

$$h(\vec{r}_{12}) = c(\vec{r}_{12}) + \rho \int c(\vec{r}_{13}) c(\vec{r}_{23})\, \mathrm{d}\vec{r}_3 + \rho^2 \int c(\vec{r}_{13})\, c(\vec{r}_{24})\, c(\vec{r}_{34})\, \mathrm{d}\vec{r}_3 \mathrm{d}\vec{r}_4 + \ldots\ldots \tag{14}$$

Next, we assume that the direct correlation functions are given by:

$$\begin{gathered} c(\vec{r}_{12}) = e^{\frac{-u(\vec{r}_{12})}{kT}} > 0 \;\; ; \;\; c(\vec{r}_{13}) = e^{\frac{-u(\vec{r}_{12})}{kT}} \left(e^{\frac{-u(\vec{r}_{13})}{kT}} - 1 + e^{\frac{-u(\vec{r}_{23})}{kT}} \right) \\ c(\vec{r}_{23}) = e^{\frac{-u(\vec{r}_{12})}{kT}} \left| e^{\frac{-u(\vec{r}_{23})}{kT}} - 1 \right| \end{gathered} \tag{15}$$

The substitution of Eqs (15) into Eq (14) leads to an equation that cannot be analytically solved. However, we search an approximate RDF which depends only on the distance between molecules, density, temperature and polarization effects [2], [15]. Hence considering only the interaction between three molecules, the following approximation follows from Eqs (9), (14) and (15):

$$g(r,\rho,T) \approx e^{\frac{-u(r,T)}{kT}} \left\{ 1 + \rho \int \left[\left(e^{\frac{-u(r,T)}{kT}} - 1 \right)^2 + \left| e^{\frac{-u(r,T)}{kT}} \left(e^{\frac{-u(r,T)}{kT}} - 1 \right) \right| \right] \mathrm{d}r^3 \right\} \tag{16}$$

To take into account the polarization in an analogous way to that of Eq (5), the term $\left|e^{-u(r,T)/kT}-1\right|$ of Eq (16) is substituted by $\left|e^{-u_M(r)/kT}-1\right|$ to approximate the radial distribution function as:

$$g(r,\rho,T)\approx e^{\frac{-u(r,T)}{kT}}\left\{1+\rho\int\left[\left(e^{\frac{-u(r,T)}{kT}}-1\right)^2+\left|e^{\frac{-u(r,T)}{kT}}\left(e^{\frac{-u_M(r)}{kT}}-1\right)\right|\right]\mathrm{d}r^3\right\} \qquad (17)$$

so that the effects of three-molecule interaction and polarization can be considered separately. The previous approximation relies on the idea that the potential $u_M(r)$ is small and hence the factor $\left|e^{-u_M(r)/kT}-1\right|$ will be very small at high temperatures, at which the polarization effect are expected to be negligible.

In addition, it is assumed that at each temperature T the integrand of Eq (17) is approximately constant for a given temperature in a volume $V_f(T)$ around three interacting molecules, so that the approximate RDF can be expressed as:

$$g(r,\rho,T)=e^{-u(r,T)/kT}\left\{1+\rho f V_f(T)\left[e^{-u(r,T)/kT}-1\right]^2+\rho V_f(T)\left|e^{-u(r,T)/kT}\left[e^{-u_M(r)/kT}-1\right]\right|\right\} \qquad (18)$$

where f is an adjustable parameter close to the unity for the calculation of C. The first term in the right-hand side of Eq (18) accounts for interactions between two molecules, whereas the second and third terms approximate the interactions between three molecules considering polarization. The volume $V_f(T)$ is defined as:

$$V_f(T)=4\pi f_g(T)\sigma^3=4\pi\int_0^\infty\left[e^{-\left[u_{POI}(r)+u_M(r)\right]/kT}-1\right]^2 r^2\mathrm{d}r \qquad (19)$$

where σ is the parameter of the Lennard-Jones potential (Eq (A2)), $u_{POI}(r)$ denotes any intermolecular potential, $u_M(r)$ is given by Eq (7) and $f_g(T)$ is a variable factor that depends on temperature and can be calculated once the intermolecular potential is chosen.

The integrand of Eq (19) is similar to the square of the Mayer function given in Eq (12). It should be noted that if the polarization effect is not considered (i.e. $u_M(r) = 0$ case of two-molecule interaction), by hypothesis when $r < r_c$ the potential $u_{POI}(r)$ will be infinite, and consequently the value of $\left[e^{-u_{POI}(r)/kT} - 1\right]^2$ will be the unit for values of $r < r_c$ where r_c is the value for which the intermolecular potential $u_{POI}(r)$ is zero [15]. According to Eqs (18) and (19), the approximate RDF can be expressed as a function of the mass density ρ_m as:

$$g\left(r,\rho_m,T\right) = e^{-u(r,T)/kT}\left\{1 + N_g\left(T\right)\rho_m\left[e^{-u(r,T)/kT} - 1\right]^2 + N_g\left(T\right)\rho_m\left|e^{-u(r,T)/kT}\left[e^{-u_M(r)/kT} - 1\right]\right|\right\} \tag{20}$$

where $N_g(T)$ is defined in accordance with Eqs (19) and (20) as:

$$N_g\left(T\right) = 4\pi f_g\left(T\right) f\sigma^3\left(\frac{N_A}{M}\right) = 4\pi\left(\frac{N_A}{M}\right)\int_0^\infty\left[e^{-\left[u(r)\right]/kT} - 1\right]^2 r^2\mathrm{d}r \qquad u\left(r\right) = u_{POI}\left(r\right) + u_M\left(r\right) \tag{21}$$

Eqs (2), (20) and (21) altogether constitute a general equation of state (EOS) that can be used with any intermolecular potential. Substituting Eq (21) into Eq (20) and expressing the resulting equation as a compressibility factor, the equations for the second (B) and third (C) virial coefficients are obtained as:

$$B\left(T\right) = -\frac{2\pi}{3}\frac{N_A}{MkT}\int_0^\infty\left(r\frac{\partial u\left(r,T\right)}{\partial r}\right)e^{-u(r,T)/kT}r^2\mathrm{d}r$$

$$C\left(T\right) = C_1\left(T\right) + C_2\left(T\right); \qquad u\left(r,T\right) = u_{POI}\left(r\right) + \overline{u}_e\left(r,T\right)$$

$$C_1\left(T\right) = -\frac{8\pi^2}{3}\frac{N_A^2}{M^2}\frac{f_g\left(T\right)f\sigma^3}{kT}\int_0^\infty\left(r\frac{\partial u\left(r,T\right)}{\partial r}\right)e^{-u(r,T)/kT}\left[e^{-u(r,T)/kT} - 1\right]^2 r^2\mathrm{d}r \tag{22}$$

$$C_2\left(T\right) = -\frac{8\pi^2}{3}\frac{N_A^2}{M^2}\frac{f_g\left(T\right)f\sigma^3}{kT}\int_0^\infty\left(r\frac{\partial u\left(r,T\right)}{\partial r}\right)e^{-u(r,T)/kT}\left|e^{-u(r,T)/kT}\left[e^{-u_M(r)/kT} - 1\right]\right|r^2\mathrm{d}r$$

where $B(T)$ and $C(T)$ are expressed in $(\mathrm{cm}^3/\mathrm{gr})$ in $(\mathrm{cm}^3/\mathrm{gr})^2$ respectively, and $\overline{u}_e$ is the total averaged electrostatic potential for polar gases (see Appendix).

It should be noted that, with the previous approximations, the virial coefficient *C(T)* in Eq (22) has the same form as the cluster expansion given by Eqs (4) and (5). However, the adjustable parameter f_{CM} of Eq (7) has different values depending on whether *C(T)* is calculated from Eqs (5) or Eqs (22), although it must be fulfilled that:

$$C_{123}(T)+C_M(T)\approx C_1(T)+C_2(T) \tag{23}$$

In addition, in Eq (22) it is necessary to consider a translational motion quantum correction B_Q that must be added up to B to account for quantum effects (especially significant in gases, such as, He4, H_2, D_2, He3), which is given by [15]:

$$B_Q(T)=\frac{h^2}{24\pi m}\frac{N_A}{(kT)^3}\int_0^\infty e^{-u(r,T)/kT}\left(\frac{\partial u(r,T)}{\partial r}\right)^2 r^2\mathrm{d}r \tag{24}$$

where h is the Planck's constant, N_A is the Avogadro number and m is the molecule mass (Eq (24) can be applied to all rigid molecules except to asymmetric tops). The quantum contributions for the rotational and Coriolis effects are small [15] and will not be considered in this paper. It is interesting to remark that the quantum corrections are small for non-polar and polar molecules, but they become significant in quantum gases, such as, He4, as it will be discussed later.

The values of *B(T)* and *C(T)* can be calculated analytically or numerically depending on the considered intermolecular potential. An important advantage of the approximation given by Eqs (20) and (21) is that they are scalar equations, whereas Eq (6) is a multidimensional vector expression whose substitution in the pressure equation (2) is cumbersome. This advantage will be used in section 6 to estimate *B(T)* and *C(T)* from chaotic PvT data obtained from a thermodynamic model in which Eq (2) and the approximate RDF of Eqs (20) and (21) are used altogether as an equation of state. Another important aspect of the approximate RDF is that it allows to estimate the heat capacity at constant volume c_v as follows:

$$\Delta c_v = \left(\frac{\partial \Delta U}{\partial T}\right)_v = 2\pi \frac{N_A^2 \rho_m}{M^2} \int_0^\infty \left[\left(\frac{\partial u((r,T)}{\partial T} \right) g\left(r, \rho_m, T\right) + u\left(r,T\right) \left(\frac{\partial g\left(r, \rho_m, T\right)}{\partial T} \right) \right] r^2 \mathrm{d}r \quad (25)$$

$$\Delta c_v = c_v\left(T\right) - c_{v0}\left(T\right) = c_v - \left[c_{p0}\left(T\right) - R \right] \quad ; \quad c_{p0}\left(T\right) = A + BT + CT^2 + DT^3 + ET^4$$

where $c_{p0(T)}$ is the heat capacity at low pressure when the gas can be considered as ideal and the coefficients *A, B, C, D, E* are tabulated for each gas [33]. Once the heat capacity at constant volume c_v is known, the heat capacity at constant pressure c_p is calculated from Eqs (20), (21) and (25) according to:

$$c_p - c_v = \frac{Tv\beta^2}{\kappa} = \frac{T\beta^2}{\rho_m \kappa} \quad ; \quad \beta = \frac{1}{v}\left(\frac{\partial v}{\partial T}\right)_p \quad ; \quad \kappa = -\frac{1}{v}\left(\frac{\partial v}{\partial P}\right)_T \quad (26)$$

where β and κ are the isobaric expansion coefficient and the isothermal compressibility coefficient respectively. Eq (2) allows to obtain β and κ as:

$$\beta = \frac{k - \frac{2\pi}{3}\frac{N_A}{M}\frac{1}{v}\int_0^\infty \left\{ \frac{\partial}{\partial T}\left(r\frac{\partial u\left(r,T\right)}{\partial r} \right) g\left(r, \rho_m, T\right) + \left(r\frac{\partial u\left(r,T\right)}{\partial r} \right)\left(\frac{\partial g\left(r, \rho_m, T\right)}{\partial T} \right) \right\} r^2 \mathrm{d}r}{kT - \frac{2\pi}{3}\frac{N_A}{M}\frac{1}{v}\int_0^\infty \left(r\frac{\partial u\left(r,T\right)}{\partial r} \right)\left\{ 2g\left(r, \rho_m, T\right) + \frac{1}{v}\left(\frac{\partial g\left(r, \rho_m, T\right)}{\partial \rho_m} \right) \right\} r^2 \mathrm{d}r} \quad (27)$$

$$\kappa = \frac{1}{\frac{N_A}{M}\frac{kT}{v} - \frac{2\pi}{3}\frac{N_A^2}{M^2}\frac{1}{v^2}\int_0^\infty \left(r\frac{\partial u\left(r,T\right)}{\partial r} \right)\left\{ 2g\left(r, \rho_m, T\right) + \frac{1}{v}\left(\frac{\partial g\left(r, \rho_m, T\right)}{\partial \rho_m} \right) \right\} r^2 \mathrm{d}r} \quad (28)$$

As it will be discussed in section 6, the calculation of heat capacities c_v and c_p are necessary for the simulation of the real gases with the proposed general equation of state given by Eqs (2), (20) and (21).

3 Virial coefficients for neon and water steam using Mie potential and the general EOS

The results of the previous section will be applied to neon as a non-polar gas and water steam as a polar one by using the Mie potential (Eq (A1)) and including the electrostatic potential due to dipole-dipole interactions (Eq (A13)) for the water steam.

For this purpose, *B(T)* and *C(T)* will be obtained through Eqs (22) and (24) (being the latter to consider quantum effects in *B(T)*) and compared with the values obtained from the Cluster expansion method by using Eqs (3)-(5). The integrals of Eqs (3), (5) and (22) will be carried out numerically (the Monte Carlo method will be used in Eqs (3) and (5)). In addition, *B(T)* will be also calculated through an analytical equation developed by Jones [1], [34], [35] that is given by:

$$B(T) = \frac{2}{3} N_A \pi \sigma^3 F(y)$$

$$F(y) = y^{3/(n-m)} \left[\Gamma\left(\frac{n-3}{n}\right) - \frac{3}{n} \sum_{r=1}^{\infty} \Gamma\left(\frac{rm-3}{n}\right) \frac{y^r}{r!} \right] \tag{29}$$

$$y^n = \left(\frac{n}{n-m}\right)^n \left(\frac{n-m}{n}\right)^m \left(\frac{\varepsilon}{kT}\right)^{n-m}$$

where Γ is the gamma function, σ and ε are the Lennard-Jones parameters for the considered gas, n is the exponent of Mie potential and $m = 6$.

The values of B and C calculated from Eq (22) will be denoted by B_{Mie} and C_{Mie} respectively, whereas those calculated through the cluster expansion method using Eqs (3)-(5) will be denoted by $B_{Cluster}$ and $C_{Cluster}$ respectively. Furthermore, the values of B calculated from Eq (29) will be denoted by $B_{Analytic}$ and the experimental values of B and C taken from Ref [4] (at the same temperatures as the calculated values for B and C) will be displayed with asterisks.

3.1 Results for neon

The estimations of B and C for Ne are carried out by using the Mie potential $u = u_{Mie}$ given in Eq (A1). Fig 1 shows the results for B considering that the Mie potential parameters are $n = 11$, $\sigma = 2.749$ Å and $\varepsilon/k = 32.3$ K [37]. The values of $B_{Mie} + B_Q$, $B_{Cluster}$ and $B_{Analytic}$ are in very good agreement at all temperatures above the critical one ($T_c = 44.4$ K) and in turn very close to the experimental data, as shown in the zoomed region between 200 and 280 K. The quantum effects B_Q calculated with Eq (24) can be considered small, and the experimental data (denoted by Exp. Data with asterisks) are taken from Ref [4].

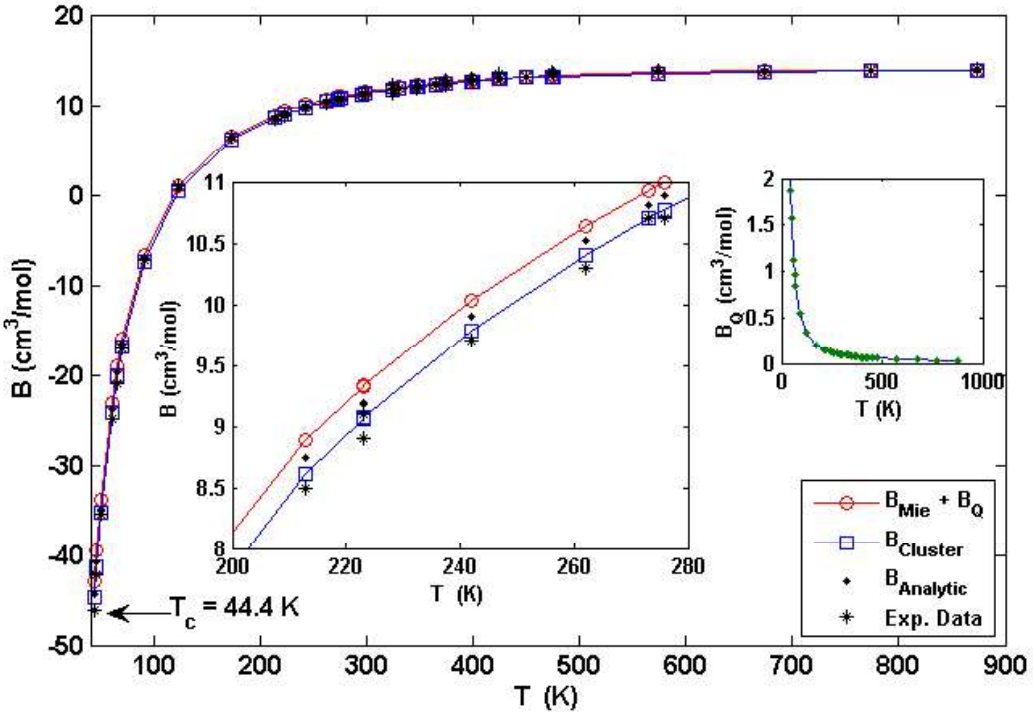

Fig 1. Results for the virial coefficient B for Ne, where B_{Mie} + B_Q is calculated through Eq (22) considering the quantum effects given by Eq (24), whereas $B_{Cluster}$ and $B_{Analytic}$ are calculated from Eqs (3) and (29) respectively. The asterisks (Exp. Data) are the experimental data for B.

The values of B_{Mie} + B_Q, B_Q, B_{Mie}, $B_{Cluster}$, $B_{Analytic}$ and the experimental ones B_{exp} are shown in table 1, whose last column contains the deviation (%) between B_{Mie} + B_Q and B_{exp}. It can be observed that the maximum deviation appears at low temperatures, especially around the Boyle temperature, although the values of $B_{Analytic}$ obtained through Eq (29) are closer to the experimental values at low temperatures. For high temperatures, the deviation is around 1 %, and the difference between B_{Mie}, $B_{Cluster}$, $B_{Analytic}$ and B_{exp} is small at all temperatures. On the other hand, the small differences between the values of $B_{Cluster}$ and $B_{Analytic}$ are due to the numerical errors associated to the calculation of the integral in Eq (22) and Monte Carlo method.

To investigate the consistency of the Mie parameters *(n, σ, ε)* we consider a similar procedure to that of Ref [16] carried out through the following steps:

i) We consider a set of values for the parameter n from $n = 8$ to $n = 40$.

ii) For each temperature T and the values of n considered in step i), $B_{Mie}(T)$ is calculated from Eq (22). Among the considered values for n, we define the best fitting value $n(T)$

as that for which $B_{Mie}(T)$ is closest to the experimental value $B_{Exp}(T)$ of B for each temperature T.

Table 1
Virial coefficients B for Ne with Mie Potential

T_{Exp} = Experimental temperatures for B from Ref [4]
B_{Mie} = Calculated with Mie potential [15], [34], [36], [37]:
$n = 11$; $\sigma = 2.749 \cdot 10^{-10}$ m; $\varepsilon/k = 32.3$ K
B_Q = Quantum correction of B [2], [15]
$B_{Cluster}$ = Calculated with the cluster expansion [2], [15]
$B_{Analytic}$ = Calculated with the gamma series expand [1], [34]
$B_{Exp} \pm \Delta B_{Exp}$ = Recommended experimental data from Ref [4]
De (%) = Deviation between $B_{Mie} + B_Q$ and B_{Exp}

T_{Exp} K	B_{Mie} cm^3/mol	B_Q cm^3/mol	$B_{Mie}+B_Q$ cm^3/mol	$B_{Cluster}$ cm^3/mol	$B_{Analytic}$ cm^3/mol	$B_{Exp}\pm\Delta B_{Exp}$ cm^3/mol	De %
46.00	-40.515	1.869	-38.645	-40.713	-40.858	-42.20±1.5	8.42
50.00	-34.544	1.581	-32.962	-34.748	-34.859	-35.40±1.4	6.88
60.00	-23.664	1.116	-22.547	-23.872	-23.927	-24.90±1.3	9.45
65.25	-19.493	0.958	-18.534	-19.701	-19.735	-21.00±1.0	11.74
70.00	-16.340	0.846	-15.494	-16.547	-16.566	-17.10±1.2	9.39
90.65	-6.947	0.547	-6.400	-7.145	-7.121	-7.20±1.0	11.11
123.15	0.791	0.339	1.131	0.604	0.663	1.00±1.0	11.59
173.15	6.450	0.207	6.657	6.284	6.359	6.50±1.0	2.36
223.15	9.260	0.146	9.406	9.107	9.189	9.10±1.0	3.26
295.00	11.365	0.101	11.446	11.223	11.311	11.20±2.0	2.32
398.15	12.779	0.068	12.847	12.648	12.739	12.90±1.0	0.40
400.00	12.693	0.068	12.761	12.666	12.756	12.70±2.0	0.48
450.00	13.162	0.058	13.221	13.035	13.127	13.20±2.5	0.52
573.15	13.659	0.043	13.703	13.538	13.631	13.80±1.0	0.70
673.15	13.832	0.035	13.868	13.715	13.809	13.70±1.0	1.22
773.15	13.899	0.030	13.930	13.785	13.879	13.90±1.0	0.22
873.15	13.904	0.026	13.931	13.792	13.886	14.00±1.0	0.49

iii) A constant reference temperature T_1 and a constant $\varepsilon/k = 32.3$ K [37] are set. For such constants and the value $n(T)$ obtained in step ii) at each temperature T, the ratio $B_{Mie}(T)/B_{Mie}(T_1)$ is obtained for different values of the parameter σ. Among the values considered for σ, we define the best fitting value $\sigma(T)$ as that for which the ratio $B_{Mie}(T)/B_{Mie}(T_1)$ is closest to the ratio $B_{Exp}(T)/B_{Exp}(T_1)$ between the experimental values of B.

iv) Step iii) is repeated with the only difference that now $\sigma = 2.749$ Å [37] is kept constant and different values for the parameter ε/k are considered. Among the values considered for ε/k, we define the best fitting value $\varepsilon(T)/k$ as that for which the ratio

$B_{Mie}(T)/B_{Mie}(T_1)$ is closest to the ratio $B_{Exp}(T)/B_{Exp}(T_1)$ between the experimental values for B.

v) The values of $\sigma(T)$ are plotted versus $\varepsilon(T)/k$ to obtain the zones of the plane defined by (ε,σ) which best fit to the experimental data.

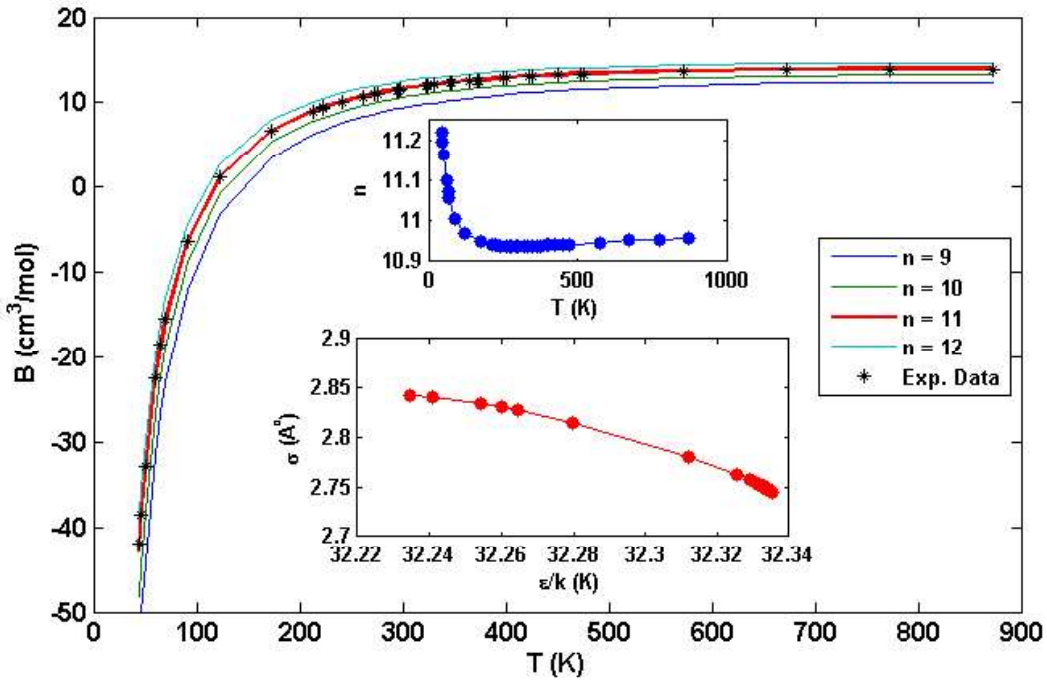

Fig 2. Virial coefficient B_{Mie} for Ne calculated from Eq (22) for the values of n indicated at the legend taking σ = 2.749 Å and ε/k = 32.3 K (continuous lines). The experimental values of B are marked with asterisks. The upper inset shows the best fitting values of n, whereas the lower inset shows the best fitting values of σ plotted versus the best fitting values of ε/k.

Fig 2 shows the results for B_{Mie} for different values of parameter n as well as the best fitting values of n and ε/k for Ne. It is corroborated that the values of n which best fit to the experimental data are very close to n = 11 for all temperatures. In addition, the variation range of ε/k is very small and σ varies in a larger range, which is in total agreement with the results of Fig 2 in Ref [36].

Fig 3 shows the values of C_1, C_2 and $C_{Mie} = C_1 + C_2$ based on the approximate RDF and calculated through Eq (22), as well as the values of $C_{Cluster}$ calculated through Eqs (3)-(5). The agreement between C_{Mie}, $C_{Cluster}$ and the experimental values of C is acceptable but worse than for the case of B, as shown in Fig 1 and Table 1. This is expectable since the expressions for $B(T)$ in Eqs (4) and (22) are equivalent [15] and the precision of the experimental data for $C(T)$ is much lower than for $B(T)$ (depending on

the experimental method, the uncertainty in B can be around 2 cm^3/mol whereas that for C can be around 50 $(cm^3/mol)^2$ [2], [4]). Furthermore, there are no experimental data for the virial coefficient C above 400 K.

The polarization effect is mainly given by the term C_2 considering the polarization intermolecular potential of Eq (7). As expected, C_2 is very small at high temperatures, at which the effects of thermal agitation are greater than those of molecular aggregation due to polarization. On the contrary, at low temperatures the polarization effects and the contribution of C_2 to C are significant.

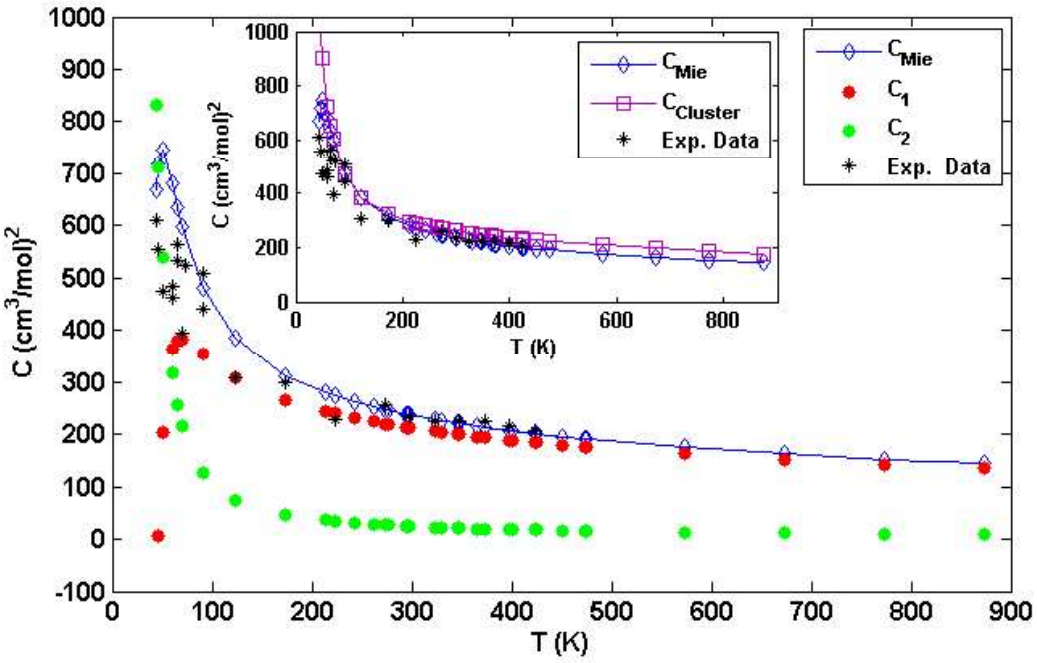

Fig 3. Results for the virial coefficient C for Ne, where C_1, C_2 and $C_{Mie} = C_1 + C_2$ are obtained from Eq (22) relying on the approximate RDF, $C_{Cluster}$ is obtained from Eqs (3)-(5) and the experimental values of C are marked with asterisks.

Table 2 shows the numerical results for the third virial coefficient C for neon. As it follows from the comparison with the results of table 1, the deviation between the calculated and experimental values for C are much higher than for B. This result is logical given that the uncertainty in the values of C is much larger than in the values of B. In general, the uncertainties of B are around 2 cm^3/mol whereas those for C are around 50 cm^6/mol^2 (although the uncertainties depend on the type of gas, temperature range and experimental method used in the determination of B and C).

Table 2
Virial coefficients C for Ne with Mie Potential

T_{Exp} = Experimental temperatures for C from Ref [4]
$C_{Mie} = C_1 + C_2$ calculated with Mie potential [2],[15], [34], [36]
$n = 11$; $\sigma = 2.749 \cdot 10^{-10}$ m; $\varepsilon/k = 32.3$ K
C_1 = Approximation of the three interaction molecules
C_2 = Approximation of the polarization effect
$C_{Cluster}$ = Calculated with the cluster expansion [2],[15]
$C_{Exp} \pm \Delta C_{Exp}$ = Recommended experimental data from Ref [4]
$f = 1$; $f_{CM} = 10$; $\alpha = 3.81 \cdot 10^{-31}$ m^3; $I_0 = 3.4543 \cdot 10^{-18}$ J
De (%) = Deviation between C_{Mie} and C_{Exp}

T_{Exp} (K)	C_1 (cm^3/mol)^2	C_2 (cm^3/mol)^2	C_{Mie} (cm^3/mol)^2	$C_{Cluster}$ (cm^3/mol)^2	$C_{Exp} \pm \Delta C_{Exp}$ (cm^3/mol)^2	*De* (%)
44.00	-146.8142	757.9907	611.1765	1050.128	610±36	0.192
46.00	6.1804	653.2872	659.4676	992.180	556±34	15.689
50.00	189.5507	502.2768	691.8275	891.650	475±30	31.341
60.00	345.0180	301.8679	646.8859	711.863	463±29	28.426
60.08	345.4869	300.8373	646.3242	710.745	483±30	25.269
65.06	364.0658	246.9924	611.0582	648.648	534±30	12.610
65.25	364.4536	245.2786	609.7321	646.544	563±50	7.664
70.00	369.3749	208.4716	577.8465	599.187	396±26	31.469
73.08	369.1518	189.5898	558.7416	573.155	523±30	6.396
90.56	350.2227	123.7310	473.9537	471.355	510±30	7.067
90.65	350.0999	123.5063	473.6062	471.097	442±50	6.673
123.15	309.7811	74.4809	384.2620	381.470	309±50	19.586
173.15	268.7283	46.7138	315.4421	322.860	299±50	5.212
223.15	242.2109	34.4639	276.6747	292.571	228±50	17.592
273.15	223.0915	27.5512	250.6426	272.454	256±30	2.092
298.15	215.2775	25.1066	240.3841	264.417	233±50	3.071
323.15	208.3177	23.0939	231.4117	257.289	224±10	3.202
348.15	202.0573	21.4064	223.4638	250.877	224±10	0.239
373.15	196.3794	19.9700	216.3494	245.044	224±10	3.415
398.15	191.1936	18.7316	209.9251	239.691	217±10	3.260
423.15	186.4287	17.6521	204.0808	234.745	208±10	1.884

3.2 Results for water steam

The estimations of B and C for water steam will be carried out by using the potential $u = u_{Mie} + u_{\mu\mu}$, where u_{Mie} is the Mie potential with parameters $n = 40$, $\sigma = 2.6410$ Å, $\varepsilon/k = 809.1$ K and $u_{\mu\mu}$ is the electrostatic dipolar potential given by Eq (A13).

Fig 4 shows that the values of B_{Mie} and $B_{Cluster}$ are both very close to the experimental data, as it can be observed in the inset for temperatures between 370 K and 430 K. However, the values of $B_{Analytic}$ obtained from Eq (29) differ from the

experimental ones and from those of B_{Mie} and $B_{Cluster}$. Such discrepancy is due to the fact that Eq (29) does not take into account the dipole-dipole interaction ($u_{\mu\mu}$), which in this case is significant due to the polar nature of water steam.

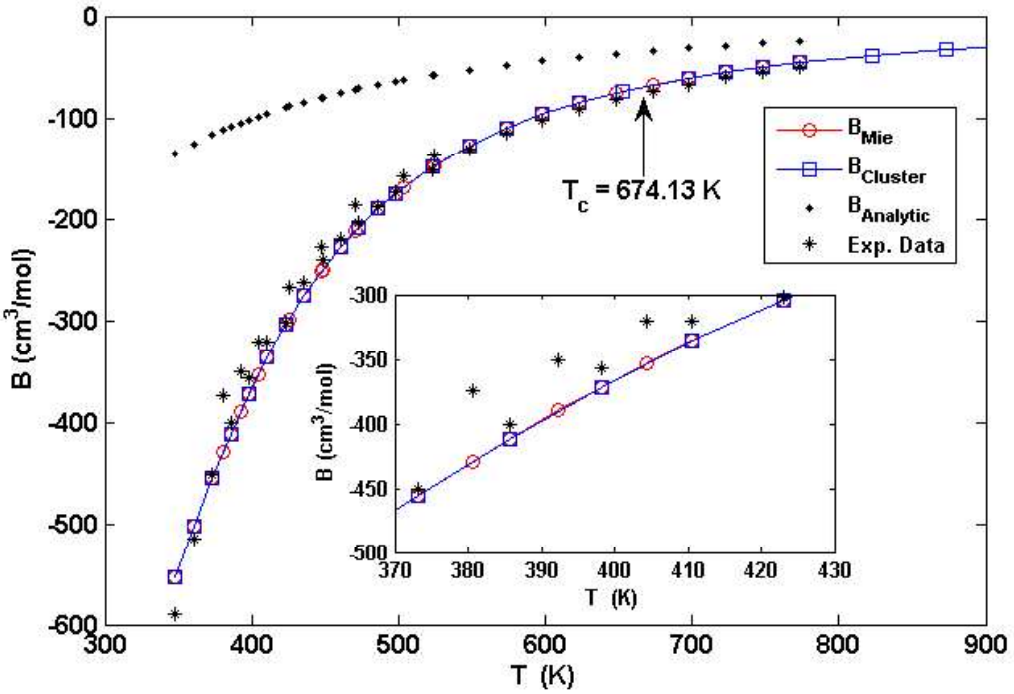

Fig 4. Results for virial coefficient B for water steam, where B_{Mie} and $B_{Cluster}$ are obtained from Eqs (22) and (3)-(5) respectively, whereas $B_{Analytic}$ is obtained through Eq (29) and the asterisks denote the experimental data for B.

Fig 5 a) shows the values of C_1, C_2 and $C_{Mie} = C_1 + C_2$ calculated through Eq (22), whereas Fig 5 b) shows the values of C_{123}, C_M and $C_{Cluster} = C_{123} + C_M$ calculated through Eqs (3)-(5). The values of C_{Mie} based on the approximate RDF are in very good agreement with the experimental data for C. In addition, the values of C_{123} and C_M are respectively different to those of C_1 and C_2. This is because C_1 and C_2 derived from the approximate RDF are not respectively equivalent to C_{123} and C_M in the cluster expansion method. However, in Figs 5 a) and b) it can be observed that $C_{Mie} = C_1 + C_2$ is approximately equal to $C_{Cluster} = C_{123} + C_M$ in accordance with Eq (23). As expected, the values of C_2 and C_M are very small at high temperatures, at which the polarization effects become negligible.

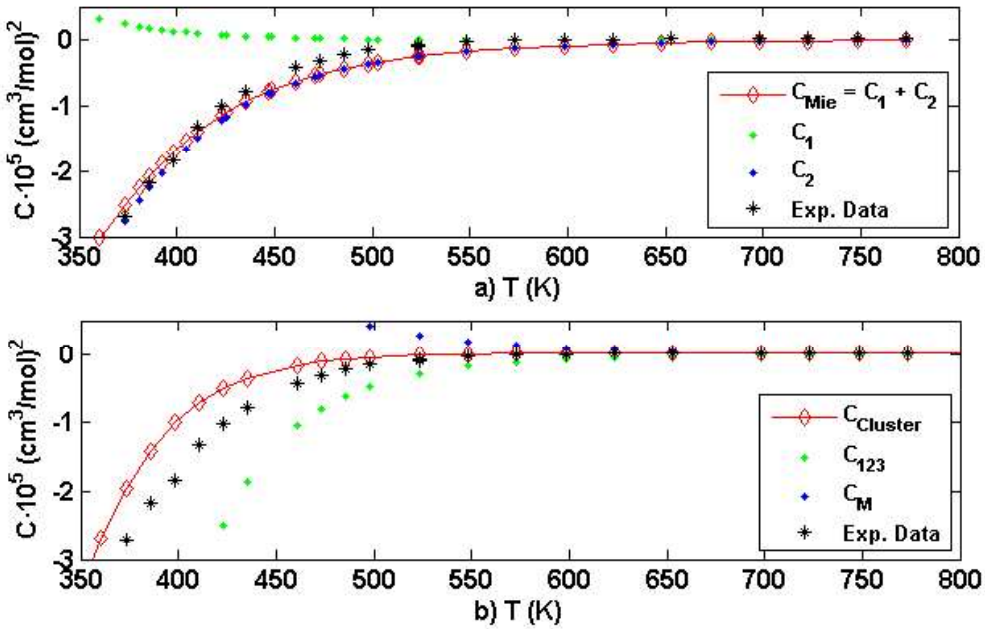

Fig 5. Results for virial coefficient C for water steam. a) Values of C_1 and C_2 and $C_{Mie} = C_1 + C_2$ obtained through Eq (22) relying on the approximate RDF. b) Values of C_{123}, C_M and $C_{Cluster} = C_{123} + C_M$ obtained through Eqs (3)-(5). The experimental data for C are marked with asterisks.

Table 3 shows the values of B_{Mie}, C_{Mie} and their deviations with respect to the respective experimental values. The deviations of B are found to be acceptable at all temperatures for which experimental data are available. The deviations of C are larger, which is expectable given the worse precision of the experimental data for C.

However, it is important to remark that the experimental data for C range between negative values of around -10^5 to positive values of approximately $7 \cdot 10^2$, and in such wide range of values the Mie potential corrected by the dipole-dipole interaction describes the trend of *C(T)*. More accurate results for *C(T)* can be obtained with empirical equations of state with more than forty parameters [38].

Table 3
Virial coefficients B and C for water steam

T_{BExp}, T_{CExp} = Experimental temperatures from Ref [4]
B_{Mie} = Calculated with Mie potential [3], [8], [15], [36], [37]
n = 40; $\sigma = 2.749 \cdot 10^{-10}$ m; ε/k = 809.1 K
C_{Mie} = Calculated with Mie potential [8], [15], [36]
$B_{Exp} \pm \Delta B_{Exp}$, $C_{Exp} \pm \Delta C_{Exp}$ = Recommended experimental data from Ref [4]
DeB(%) = Deviation between B_{Mie} and B_{exp}
DeC(%) = Deviation between C_{Mie} and C_{exp}
T_c = 674.13 K; $\alpha = 1.48 \cdot 10^{-30}$ m^3; $I_0 = 2.0203 \cdot 10^{-18}$ J; f = 1; f_{CM} = 68

T_{BExp} K	B_{Mie} cm^3/mol	$B_{Exp} \pm \Delta B_{Exp}$ cm^3/mol	DeB (%)	T_{CExp} K	$C_{Mie} \cdot 10^3$ cm^6/mol^2	$10^3(C_{Exp} \pm \Delta C_{Exp})$ cm^6/mol^2	DeC (%)
348.15	-553.64	-590.3±15	6.21	348.15	-281.17	-439±90	35.95
360.65	-503.03	-515.0±10	2.32	360.65	-238.21	-342±64	30.34
373.15	-455.40	-451.0±40	0.97	373.15	-198.20	-270±45	26.59
385.65	-428.90	-374.0±80	1.28	385.65	-163.01	-217±32	24.88
398.15	-411.50	-400.9±6.7	2.58	398.15	-133.15	-183±25	27.23
392.34	-371.66	-350.3±80	5.74	410.65	-108.38	-132±16	17.89
398.15	-371.65	-356.8±38	4.00	423.15	-88.12	-101±15	12.74
410.65	-335.65	-320.9±4.4	4.45	435.65	-71.69	-77.4±8	7.369
423.15	-303.85	-301.7±35	0.71	460.65	-47.75	-41.8±4	12.46
460.65	-227.83	-220.3±1.8	3.30	473.15	-39.14	-31.8±6	18.75
485.65	-175.42	-188.1±1.9	6.74	485.65	-32.19	-21.5±2	33.21
523.15	-148.47	-151.8±1.3	2.19	498.15	-26.55	-18.3±1.7	31.07
573.15	-110.44	-115.6±0.3	4.46	523.15	-18.27	-10.2±0.6	44.22
598.15	-96.576	-102.0±0.3	5.31	923.15	0.583	0.82±0.2	28.90
623.15	-85.153	-91.7±0.7	7.13	1023.15	0.714	0.62±0.2	13.16
723.15	-55.103	-60.1±0.1	8.31	1073.2	0.737	0.55±0.2	25.47
773.15	-45.799	-49.8±0.2	8.03	1173.2	0.746	0.44±0.2	41.07

3.3 Nomenclature for the variables and units used in the proposed EOS

Table 4 shows the nomenclature for the variables and units used in sections 2 and 3.

Table 4
Variables used in the formulation of the EOS

Variable	Description	Units
ΔU	Variation of the gas internal energy	J
N_A	Avogadro number ($6.02214 \cdot 10^{23}$)	mol^{-1}
k	Boltzmann constant ($1.38066 \cdot 10^{-23}$)	$J \cdot K^{-1}$
P	Pressure of the EOS	$N \cdot m^{-2}$
M	Molecular mass of the gas	$kg \cdot mol^{-1}$
ρ	Gas density	m^{-3}
ρ_m	Gas mass density	$kg \cdot m^{-3}$
r	Distance between atoms	m
T	Gas temperature	K
$g(\rho,r,T)$	Radial distribution function RDF	
$B(T)$	Second virial coefficient	$cm^3 \cdot mol^{-1}$
$B_Q(T)$	Quantum effects in the second virial coefficient	$cm^3 \cdot mol^{-1}$
h	Planck constant ($6.626 \cdot 10^{-34}$)	$J \cdot s$
$C(T)$	Third virial coefficient	$cm^6 \cdot mol^{-2}$
$C_{123}(T)$	Contribution to three-molecule interactions	$cm^6 \cdot mol^{-2}$
$C_M(T)$	Contribution due to the polarization effect	$cm^6 \cdot mol^{-2}$
u_{ij}	Interaction potential between molecules i and j	J
f_{ij}	Mayer function	
V_e	Integration volume for determining $g(r,\rho,T)$	m^3
$u_M(\theta_{ijk},r_{ij})$	Intermolecular potential due to the polarization	J
$u_{POI}(r)$	Any intermolecular potential of Appendix	J
$u_M(r)$	Approximation of $u_M(\theta_{ijk},r_{ij})$	J
$u(r)$	Intermolecular potential $u_{POI}(r) + u_M(r)$	J
f_{CM}	Variable factor in the calculation of $u_M(r)$	
f_M	Mayer function associated to the potential $u_M(r)$	
α	Polarizability of the gas	m^3
I_0	First ionization potential of the gas	J
$h(r_{ij})$	Correlation function between molecules i and j	
$c(r_{ij})$	Direct correlation function for molecules i and j	
f	Factor to approximate the RDF	
$g_i(r,T)$	Interaction of three ($i=1$) and four ($i=2$) molecules	
$f_g(T)$	Parameter to approximate $g(r,\rho,T)$	
$V_f(T)$	Integration volume to approximate $g(r,\rho,T)$	m^3
$N_g(T)$	Parameter to approximate $g(r,\rho,T)$	
$C_1(T)$	Part of $C(T)$ due to three-molecule interactions	$cm^6 \cdot mol^{-2}$
$C_2(T)$	Part of $C(T)$ due to the polarization effect	$cm^6 \cdot mol^{-2}$
σ	Lennard-Jones parameter	m
ε	Lennard-Jones parameter	J
Γ	Gamma function	
y	Parameter in the $B(T)$ expansion	
$F(y)$	Function of the parameter y	
β	Isobaric expansion coefficient	K^{-1}
κ	Isothermal compressibility coefficient	$(N/m^2)^{-1}$
$c_{p0}(T)$	Heat capacity of the gas considered as ideal	$J/(kg \cdot K)$

4 Thermodynamic model to obtain PvT chaotic data by using the general EOS

As it was discussed in section 2, Eq (2) and the approximate radial distribution function (RDF) given by Eqs (20) and (21) altogether define a general equation of state (EOS) that can be used with any real gas and intermolecular potential. In this section, such general EOS is applied in the context of the thermodynamic model shown in Fig 6, which is ultimately aimed to achieve a chaotic behavior of the pressure P and specific volume v while keeping an almost constant temperature T. With such behavior, the virial coefficients $B(T)$ and $C(T)$ can be estimated from the simulated PvT values, since the chaotic behavior collects the dynamical properties of each considered gas [16]. By comparing the values of B and C estimated from chaotic PvT data with the experimental values of B and C it is possible to elucidate the pressure and temperature ranges at which $B(T)$ and $C(T)$ have a significant contribution on the virial equation given by [4], [14], [15]:

$$z=\frac{Pv}{RT}=1+\frac{B(T)}{v}+\frac{C(T)}{v^2}+\ldots.\ ;\quad v\left(\frac{Pv}{RT}-1\right)=B(T)+\frac{C(T)}{v} \tag{30}$$

where T is the temperature, P is the pressure, $v = 1/\rho$ is the specific volume (being ρ the density) and only $B(T)$ and $C(T)$ will be considered since the experimental data for the rest of virial coefficients are inaccurate or unknown. For instance, at very low pressures the specific volume v is very large and hence $B(T)$ and $C(T)$ do not have an appreciable effect in Eq (30), i.e., $z \approx 1$ and the gas can be regarded as approximately ideal. However, as the pressure increases and v decreases, $B(T)$ and $C(T)$ gain relevance in Eq (30).

To estimate the virial coefficients from the PvT values, the thermodynamic model is numerically simulated using the general EOS of Eqs (2), (20) and (21) in a chaotic regime for P and v while keeping an almost constant temperature T. In this regime, $B(T)$ and $C(T)$ are obtained as the values that best fit to the linear equation $y = B(T) + C(T)x$ being $y = v[Pv/(RT)-1]$ and $x = 1/v$, which is carried out by using the least square method. The comparison of $B(T)$ and $C(T)$ estimated from the PvT values with the experimental data for $B(T)$ and $C(T)$ also allows elucidating to what extent a given intermolecular potential reproduces the behavior of a gas in a certain range of

temperatures and pressures. This provides a procedure to analyze different intermolecular potentials for different gases at different temperature and pressure ranges with the proposed general EOS, and hence without the need to resort to empirical EOS.

The thermodynamic model of Fig 6 includes an input and output gas flow and two proportional plus integral action controllers PI_1 and PI_2, whose tuning parameters are constant [17-20]. The accumulation vessel has a coil that supplies the heating-cooling heat flow *Q(t)* to maintain a constant gas temperature so that Eq (30) can be used to estimate *B(T)* and *C(T)* from the PvT values. In addition, it is assumed that the coil is designed so that the heat flow is proportional to the flow rate $F_v(t)$. When the servo-valve CV2 is closed the gas temperature in the vessel varies in accordance with the inlet pressure *P(t)* and the inlet mass flow rate $\dot{m}_d(t)$, which can be modified by means of the valve V_2.

It is assumed that the sensors of temperature S_T, pressure S_P and the transmitters PT and TT provide information on the gas pressure *P(t)* and temperature *T(t)*, whereas the flow rates $F_2(t) = \dot{m}_2(t)/\rho_2(t)$ and $F_s(t) = \dot{m}_s(t)/\rho(t)$ are measured at each instant. From this information and the EOS of Eqs (2), (20) and (21), the device generates the electric signal f(t) that opens or closes the servo-valve CV2 to obtain an adequate heating-cooling flow rate $F_v(t)$. Furthermore, a pressure probe is used to measure the output pressure $P_2(t)$ of the servo-valve CV1, which is connected to a reservoir to expel the gas.

The desired set pressure P_d and the output pressure of the control valve $P_2(t)$ are transformed into adequate electric currents i_s and *i(t)* through the converter K_t, which in turn generates the force *F(t)* in the servo-valve CV1 [17-20]. Next, we shall define the equations of the mechanical subsystem formed by the servo-valve CV1 and the controller PI_1 [16].

i) Model of valve CV1 and controller PI_1

The valve plug is modeled as a mass *m* with a damping coefficient δ ($0 < \delta < 1$), a nonlinear spring and a nonlinear term that represents the nonlinearities associated to

the valve deformation and non-modeled dynamics. The dimensionless plug displacement $x(t)$ is expressed as a fraction of the maximum displacement x_{max} and hence $0 \le x(t) \le 1$. The undamped natural frequency is given by ω_n and it is assumed that the force $F(t)$ applied on the valve plug is related to the current $i_{PI}(t)$ in the electro-valve-solenoid through the constant K_a expressed in N/mA. The global equations can be defined as [16]:

$$\frac{dx_1(t)}{dt} = x_2(t) \;\; ; \;\; \frac{dx_2(t)}{dt} = x_3(t)$$
$$\frac{dx_3(t)}{dt} = -\omega_n^2 x_2(t) - 2\delta\omega_n x_3(t) + K_t\left[P_d - P_2(t)\right] - \frac{K_{NL}}{\tau_i} x_1^2(t) x_2(t) \qquad (31)$$
$$x(t) = b_0 x_1(t) + b_1 x_2(t)$$

The parameters b_0, and b_1 and the proportional constant of the controller K_c are defined as:

$$b_0 = \frac{K_a K_c}{m x_{\max}} \frac{K_0}{\tau_I} \;\; ; \; b_1 = \frac{K_a K_c K_1}{m x_{\max}} \;\; ; \; K_c = \frac{100}{PB} \qquad (32)$$

where K_c is the proportional constant of the PI controller defined from its proportional band PB as $K_c = 100/PB$, K_1 and K_0 are respectively adjustable dimensionless constants for the proportional and integral actions, τ_i is the reset time, K_t $(mA \cdot m^2/N)$ is the transmitter constant (the current is measured in milliamps), P_d is the desired pressure for the PI_1 controller and $P_2(t)$ is the measurement of the pressure probe (see Fig 6).

The values and units of the parameters indicated in Eq (32) are $m = 5 \cdot 10^{-2}$ kg, $x_{max} = 0.01$ m, $K_a = 0.3125$ N/mA, $PB = 50$ and $\tau_i = 300$ s [17-19], for which it is obtained that $b_0 = 4.1667 \cdot K_0$ (1/mA·s^3) and $b_1 = 1250 \cdot K_1$ (1/mA·s^3). The dimensionless parameters K_0 and K_1 are chosen so that $b_0 >> b_1$. In particular, $K_0 \approx 1.9$ and $K_1 \approx 6.5 \cdot 10^{-5}$ can be considered as admissible values for the numerical simulations.

As it will be discussed later, the values of K_{NL} in Eq (31) are chosen to obtain self-oscillation conditions according to:

$$K_{NL}/\tau_I = K_{NLd} f_{KNL}/\tau_I \;\; ; \;\; K_{NLd} = 8.4146 \cdot 10^{-4} \;\; \left(1/\text{mA}^3.s^8\right) \;\; ; \;\; 1 < f_{KNL} < 10^8 \qquad (33)$$

where f_{KNL} is a constant factor whose value will allow to obtain different dynamical behaviors and K_{NLd} is a convenient reference value.

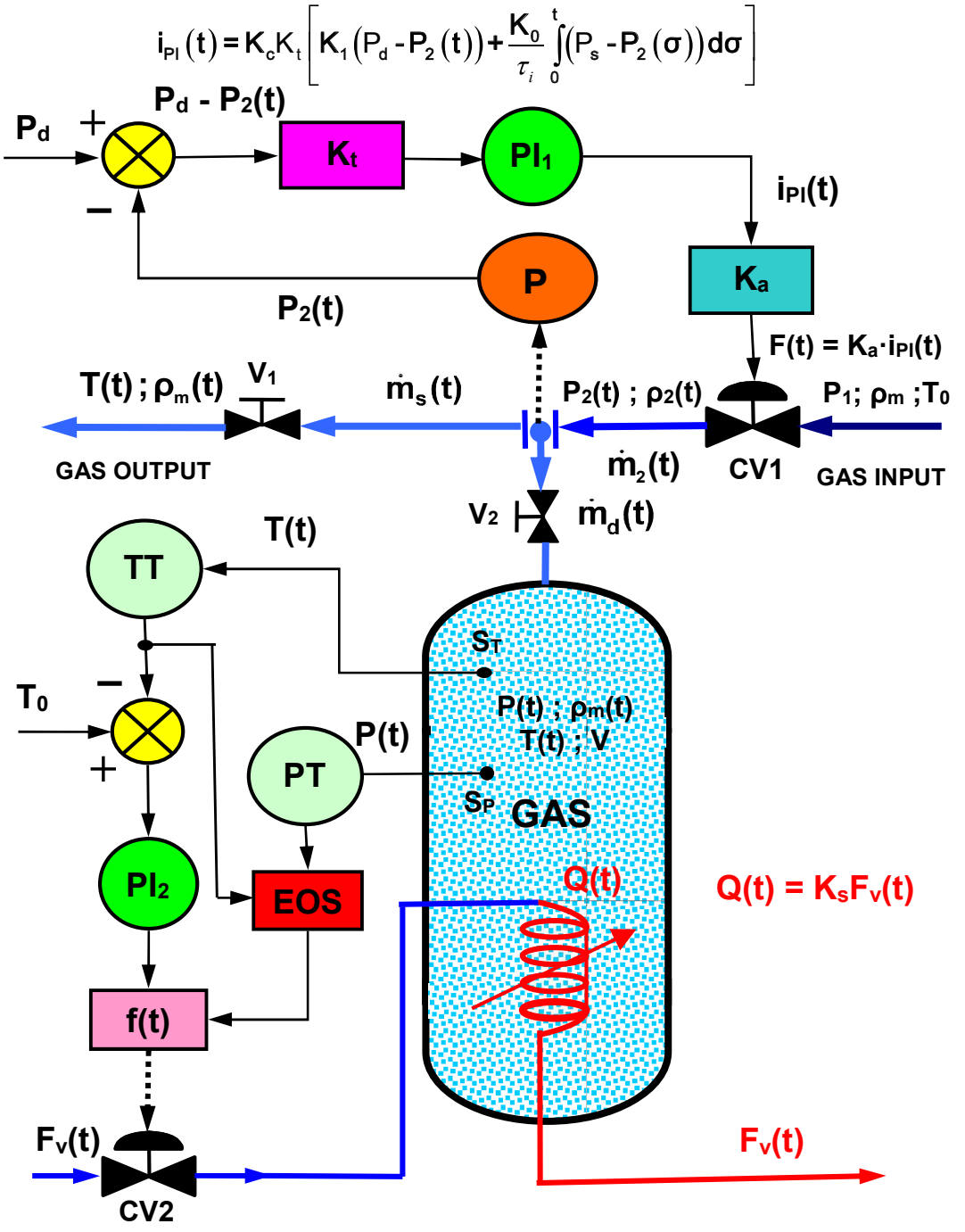

Fig 6. Thermodynamic model which includes controllers PI_1 and PI_2, servo-valves CV1 and CV2, pressure probe P, temperature and pressure sensors S_T and S_P, transmitters of temperature TT and pressure PT, converters of pressure K_t and current K_a, pipes, auxiliary valves, an accumulation vessel and a heating-cooling coil. The force F(t) produces the movement of the servo-valve CV1 whereas the force f(t) generates the plug movement of the servo-valve CV2 (EOS refers to the proposed general equation of state).

ii) Flow rate in the servo-valve CV1

The model of the flow rate relies on the assumption of isentropic flow [21]. The mass flow rate $\dot{m}_2(t)$ (kg/s) is related to the flow rate $F_2(t)$ (m^3/s) according to:

$$F_2(t)=\frac{\dot{m}_2(t)}{\rho_2(t)}=\begin{cases}\sqrt{\frac{2}{R}}\frac{C_f A_0 f\left[x(t)\right]}{\rho_2(t)}\frac{\varepsilon}{\sqrt{T_0}}\sqrt{P_2(t)\left[P_1-P_2(t)\right]} \\ \varepsilon=0.97+0.0636\left(\frac{P_2(t)}{P_1}-0.528\right);\ \text{for}\ \frac{P_{ch}}{P_1}>\left(\frac{2}{k+1}\right)^{k/k-1} \\ \frac{C_f A_0 f\left[x(t)\right]}{\rho_2(t)}\frac{P_1}{\sqrt{RT_0}}\cdot\sqrt{k\left(\frac{2}{k+1}\right)^{k+1/k-1}}\ ;\ \text{for}\ \frac{P_{ch}}{P_1}\le\left(\frac{2}{k+1}\right)^{k/k-1}\end{cases} \quad (34)$$

In Eq. (34), ε is the so called expansion coefficient, C_f is the valve discharge coefficient ranging between 0.68 and 0.9, A_0 =$4\cdot10^{-6}$ m^2 is a characteristic area of the valve, T_0 is the inlet gas temperature and $k = c_p(T)/c_v(T)$, where $c_p(T)$ and $c_v(T)$ are respectively the heat capacity at constant pressure and volume calculated with Eqs (2), (20), (21) and (25)-(28). In addition, R is the gas constant, P_1 and $P_2(t)$ are the respective input and output pressures and P_{ch} is the critical pressure at which the flow is choked when $P_2(t) \equiv P_{ch}$, i.e., $\dot{m}_2(t)=F_2(t)\rho_2(t)$ remains constant for $P_{ch}\le(2/k+1)^{k/k-1}P_1$. This means that if the downstream pressure is below P_{ch} then the gas velocity is sonic and the pressure $P_2(t)$ has no influence on the mass flow of the gas. In addition, the value of the plug position $x(t)$ and $f[x(t)]$ for a linear valve are given by [20-25]:

$$f\left[x(t)\right]=x(t)=b_0x_1(t)+b_1x_2(t) \quad (35)$$

iii) Model of the pressure probe and servo-valve

The output pressure $P_2(t)$ of the servo-valve CV1 is assumed to fulfill the first order differential equation given by:

$$T_m \frac{\mathrm{d}P_2(t)}{\mathrm{d}t} + P_2(t) = K_m F_2(t) \tag{36}$$

where T_m is a time constant with admissible values between 5 and 10 seconds and K_m $(\mathrm{N \cdot m^{-2}})/(\mathrm{m^3 \cdot s^{-1}})$ is a constant parameter defined in terms of the input pressure P_1 as:

$$K_m = \frac{2 \cdot 10^8 P_1}{10^5 f_{Km}} \;\; ; \;\; 1 \le f_{Km} \le 4 \tag{37}$$

where it is assumed that a pressure $P_1 = 10^5$ $\mathrm{N/m^2}$ corresponds to $K_m = 2 \cdot 10^8$ $(\mathrm{N \cdot m^{-2}})/(\mathrm{m^3 \cdot s^{-1}})$ if $f_{Km} = 1$, where f_{Km} is a factor that can take values between 1 and 4.

iv) Model of the thermal subsystem

Considering the scheme of Fig 6 and assuming that the gas density in the output pipe is equal to the gas density within the vessel, the mass balance in the accumulator vessel can be written as:

$$V \frac{\mathrm{d}\rho_m(t)}{\mathrm{d}t} = \dot{m}_2(t) - \dot{m}_s(t) \;\; ; \;\; \begin{cases} \dot{m}_2(t) = F_2(t)\rho_2(t) \\ \dot{m}_s(t) = F_s(t)\rho_m(t) \end{cases} \tag{38}$$

where V is the vessel volume, $\rho_m(t)$ $(\mathrm{kg/m^3})$ is the density of the gas within the vessel and $\dot{m}_2(t)$ and $\dot{m}_s(t)$ (kg/s) are the mass flow rates in the input and output pipes respectively. On the other hand, assuming that the heat losses and the stored heat in the vessel walls are both negligible and recalling that $F_v(t)$ is a heating-cooling flow rate in the servo-valve CV2, the energy balance for the gas in the vessel is given by:

$$\frac{\mathrm{d}T(t)}{\mathrm{d}t} = \frac{\rho_2(t)F_2(t)\left[c_p(T)T_0 - c_v(T)T(t)\right] - \rho_m(t)F_s(t)T(t)\left[c_p(T) - c_v(T)\right] + K_s F_v(t)}{V c_v(T)\rho_m(t)} \tag{39}$$

where K_s is a constant that depends on the heating-cooling coil design. Besides Eqs (38) and (39), it is necessary to consider the following mass balance at the output of the valve CV1 (see Fig 6):

$$\dot{m}_2(t) = \dot{m}_d(t) + \dot{m}_s(t) \Rightarrow \rho_2(t) F_2(t) = \rho_2(t) F_d(t) + \rho_m(t) F_s(t) \tag{40}$$

where $F_d(t)$ is the gas flow rate to the vessel regarded as positive when the gas enters the vessel and negative when the gas leaves the vessel, whereas the densities $\rho_2(t)$ and $\rho(t)$ are obtained from the EOS of Eqs (2), (20) and (21). The flow rate $F_d(t)$ is modeled as:

$$F_d(t) = \begin{cases} K_d \sqrt{P_2(t) - P(t)} & \text{if } P_2(t) > P(t) \\ K_d \sqrt{P(t) - P_2(t)} & \text{if } P(t) > P_2(t) \end{cases} \tag{41}$$

where K_d can be considered as a discharge coefficient of the valve V_2 that ranges from 10^{-7} to $9 \cdot 10^{-7}$ $(m^3/s)/(N/m^2)^{0.5}$. It will be assumed that valve CV2 remains closed (i.e., $F_v(t) = 0$) until it is opened at an arbitrary time $t = t_C$ with a flow rate $F_v(t)$ defined as:

$$K_s F_v(t) = -\rho_2(t) F_2(t) \left[c_p(T) T_0 - c_v(T) T(t) \right] + \rho_m(t) F_s(t) T(t) \left[c_p(T) - c_v(T) \right] + \\ + V c_v(T) \rho_m(t) \left\{ 2 \delta_T \omega_{nT} \left[T_0 - T(t) \right] + \omega_{nT}^2 \int_0^t \left[T_0 - T(\sigma) \right] \mathrm{d}\sigma \right\} \tag{42}$$

where $\rho_2(t)$ is obtained from P_1 and T_0 by means of the proposed general EOS and the gas pressure $P_2(t)$ is measured by the pressure probe. The temperature $T(t)$ and pressure $P(t)$ of the gas in the vessel are measured by the sensors S_T and S_P, so the gas density in the vessel $\rho(t)$ can be calculated from the general EOS. The parameters δ_T and ω_{nT} are chosen to obtain the desired gas temperature T_0 in the vessel. For this purpose, substituting Eq (42) into Eq (39) and differentiating with respect to time we obtain a second order linear differential equation whose general solution for $0 < \delta_T < 1$ is given by [21]:

$$\frac{\mathrm{d}^2T(t)}{\mathrm{d}t^2}+2\delta_T\omega_{nT}\frac{\mathrm{d}T(t)}{\mathrm{d}t}+\omega_{nT}^2T(t)=\omega_{nT}^2T_0$$
$$T(t)=T_0+\frac{\exp\left(-\delta_T\omega_{nT}t\right)}{\sqrt{1-\delta_T^2}}\sin\left[\omega_{nT}\sqrt{1-\delta_T^2}t+\Phi\right] \tag{43}$$

where Φ is an arbitrary phase that depends on the initial conditions. It is clear that the gas temperature $T(t)$ tends to T_0 as $t\to\infty$ with a rapidity that depends on the chosen values for δ_T and ω_{nT}. Consequently, the energy balance can be defined as:

$$\begin{cases}\dfrac{\mathrm{d}T(t)}{\mathrm{d}t}=\dfrac{\rho_2(t)F_2(t)}{Vc_v\rho_m(t)}\left[c_p(T)T_0-c_v(T)T(t)\right]-\dfrac{\rho_m(t)F_s(t)T(t)}{Vc_v\rho_m(t)}\left[c_p(T)-c_v(T)\right] & \text{for } t\le t_C\\ \dfrac{\mathrm{d}^2T(t)}{\mathrm{d}t^2}+2\delta_T\omega_{nT}\dfrac{\mathrm{d}T(t)}{\mathrm{d}t}+\omega_{nT}^2T(t)=\omega_{nT}^2T_0 & \text{for } t>t_C\end{cases} \tag{44}$$

Eqs (38)-(44) altogether constitute the model of the thermal subsystem.

v) Self-oscillating and chaotic behaviors

The equilibrium points of the system are necessary to obtain the self-oscillating and chaotic behavior, which in turn is required to obtain the virial coefficients of the gas. Assuming that $F_v(t) = 0$ (i.e., the heating-cooling system is off) and taking into account that the derivatives of the variables $x_1(t)$, $x_2(t)$, $x_3(t)$, $P_2(t)$, $\rho_m(t)$ and $T(t)$ are zero at equilibrium, from Eqs (31), (39) and (44) it is deduced that:

$$P_d/K_m=\sqrt{2/R}\left(C_fA_0/\rho_{2e}\right)\left(\varepsilon_e x_e/\sqrt{T_0}\right)\sqrt{P_d\left(P_1-P_d\right)}\ ;\ f\left(x_{1e}\right)=x_{1e}=x_e/b_0 \tag{45}$$

where P_d is the desired pressure and ρ_{2e} is the gas density at equilibrium determined from the general EOS given by Eqs (2), (20) and (21). It should be noted that once P_d is fixed, Eq (45) allows to obtain the dimensionless plug valve position $x_{1e} = x_e$.

The previously derived mathematical model for Fig 6 implies a one-way coupling from the mechanical subsystem to the thermal one. This means that the

mechanical system influences the thermal one, but the latter has no influence on the former, so the self-oscillating conditions can be considered for the mechanical subsystem only. For this purpose, the system equations can be expressed in deviation variables as detailed in Ref [16]. The characteristic polynomial of the matrix of the linear part of the system around the equilibrium point is a fourth order polynomial of that can be written as:

$$P(s) = s^4 + a_3 s^3 + a_2 s^2 + a_1 s + a_0$$

$$a_3 = 2\delta\omega_n - B \;\; ; \;\; a_2 = \omega_n^2 + \frac{K_{NL}}{\tau_i} x_{1e}^2 - 2\delta\omega_n B \;\; ; \;\; a_1 = b_1 A K_t - \left(\omega_n^2 + \frac{K_{NL}}{\tau_i} x_{1e}^2 \right) B \;\; ; \;\; a_0 = b_0 A K_t$$

$$a_{23} = \left(\omega_n^2 + \frac{K_{NL}}{\tau_i} x_{1e}^2 \right) ; Ab_0 = \left(\frac{\partial F_2}{\partial x_1} \right)_e \;\; ; Ab_1 = \left(\frac{\partial F_2}{\partial x_2} \right)_e \;\; ; B = \left(\frac{\partial F_2}{\partial P_2} \right)_e \tag{46}$$

where the sub index e means equilibrium.

The self-oscillation condition is sought by imposing the condition that the characteristic polynomial *P(s)* has two complex conjugate roots (weak focuses) [39], [40], [41] and the other two roots have a negative real part, so it is obtained that:

$$a_1 a_2 a_3 - a_1^2 = a_0 a_3^2 \tag{47}$$

The next step is to determine the values of K_{NL} which provide weak focuses associated to the self-oscillating behavior. For this purpose, we observe that the values of a_0 and a_3 in Eqs (47) are independent of K_{NL}, so the self-oscillating condition can be written as a second-degree polynomial in terms of a_{32} according to:

$$a_1 a_2 a_3 - a_1^2 = a_0 a_3^2 \;\; ; \;\; a_{32} = \omega_n^2 - \left(K_{NL} / \tau_I \right) x_{1e}^2 \Rightarrow a_1 a_2 a_3 - a_1^2 - a_0 a_3^2 = P\left(a_{23}\right) = 0$$

$$P\left(a_{32}\right) = -B\left(a_3 + 1\right) a_{32}^2 + \left[\left(b_1 A K_t - 2\delta\omega_n B^2 \right) a_3 + 2 b_1 A K_t B \right] a_{32} - \tag{48}$$

$$2\delta\omega_n B b_1 A K_t a_3 - \left(b_1 A K_t \right)^2 - a_0 a_3^2 = 0$$

Eqs (48) allows to obtain the positive root *PR[P(a23)]* of *P(a23)*, for which the value $K_{NL} = K_{NLos}$ in Eq (33) to obtain a weak focus is given by:

$$K_{NLos} = \frac{\left\{PR\left[P\left(a_{23}\right)\right] - \omega_n^2\right\}\tau_I}{x_{1e}^2} \tag{49}$$

where ω_n^2 must be chosen so that $PR\left[P\left(a_{23}\right)\right] - \omega_n^2 > 0$.

Once the weak focuses are determined, the simulation values of K_{NL} are calculated by taking a set of values for a dimensionless constant f_{KNLos} so that $K_{NL} = K_{NLos} = f_{KNLos} \cdot K_{NLd}$ (Eq (49)).

The self-oscillating behavior provides a route to obtain the desired PvT chaotic oscillations. It is well known that a harmonic disturbance in a system parameter can lead to chaotic dynamics [39], [40] when the matrix of the linearized system at the equilibrium point has a weak focus. Such harmonic disturbance will be introduced by varying harmonically the time constant of the pressure probe T_m according to:

$$T_m\left(t\right) = T_{ma} + AT_m \sin\left(\omega_{Tm} t\right) \tag{50}$$

where AT_m and ω_{Tm} are the amplitude and the angular frequency respectively, and in addition it must be fulfilled that $T_{ma} > AT_m$.

5 Simulation of the thermodynamic model for the estimation of B and C

To estimate the virial coefficients B and C by means of Eq (30) using the PvT values obtained from the numerical simulation of the thermodynamic model of Fig 6, two conditions must be met. On one hand, the simulated PvT values must have a high enough variability so that their adjustment with the least square method is reliable. On the other hand, Eq (30) is valid at each constant temperature T, so each estimation of B and C must be done at an approximately constant temperature.

The first step in the simulation of the model of Fig 6 consists of setting a pressure P_1 and a temperature T_0 at the device inlet for the considered gas without entering the biphasic zone. Once P_1 and T_0 have been set, a desired pressure P_d ($P_d < P_1$) is defined so that the controller PI_1 gives rise to a system equilibrium point at the pressure P_d and at the gas input temperature T_0. In equilibrium it must be fulfilled that

$P_2(t) \equiv P_d$, so from Eqs (45) it follows that $x_{2e} = 0$, $x_{3e} = 0$ and in addition $\dot{m}_2(t) = \dot{m}_s(t)$ as per Eqs (38). On the other hand, from Eqs (40) and (41) it follows that $\dot{m}_d(t) = 0 \Rightarrow F_d(t) = 0$, so the gas pressure in the accumulator vessel must be $P(t) \equiv P_d$.

Since in equilibrium it must be fulfilled that $dT(t)/dt = 0$, Eqs (39) and (42) imply that $T(t) \equiv T_0$, and from Eqs (39) and (45) the equilibrium values ρ_e for the gas density and x_{1e} for the variable $x_1(t)$ can be obtained. With the equilibrium point $P_e(x_{1e}, 0, 0, \rho_e, P_d, T_0)$, the dynamical behavior of the system depends on the values of $F_v(t)$, K_{NLos} and $T_m(t)$ given by Eqs (42), (49) and (50) respectively, which allows to distinguish the following operation regimes:

i) The constant K_{NLos} does not fulfill Eq (49). In this case two dynamical behaviors may take place. On one hand, if all the roots of the characteristic polynomial given by Eq (46) have negative real part then the system is stable and will reach the equilibrium point P_e. On the other hand, if any of the roots of the characteristic polynomial of Eq (46) has positive real part then the system is unstable. None of the two previous behaviors is suitable for our purpose, since none of them can provide the desired variability for the PvT data while keeping an approximately constant temperature.

ii) The constant K_{NLos} fulfills Eq (49), $T_m(t)$ is constant with time in Eq (50) ($AT_m = 0$) and the heating-cooling system is disconnected so that $F_v(t) = 0$ (Eq (42)). In this case, the characteristic polynomial given by Eq (46) has a pair of conjugate pure imaginary roots (weak focus) and other two roots with negative real part. Consequently, the system reaches a self-oscillating behavior in which the gas pressure will oscillate around P_d. This behavior is not suitable for our purpose since the temperature will not be constant and there will not be enough variability in the PvT data, but it offers a route to a chaotic behavior in which the desired variability in the PvT data can be achieved.

iii) The constant K_{NLos} fulfills Eq (49) and the flow rate is $F_v(t) = 0$ (as in case ii)), but now $T_m(t)$ varies harmonically with time according to Eq (50). In this case the PvT simulated values can become chaotic thus achieving the desired variability. However, the chaos itself implies that the temperature will have a high variability, which is undesired for the estimation of B and C through Eq (30). This justifies the need of a

cooling-heating system that maintains the temperature of the gas in the vessel almost constant while the pressure and density of the gas oscillate chaotically.

iv) The constant K_{NLos} fulfills Eq (49) and $T_m(t)$ varies harmonically with time so that chaotic behavior is obtained (as in case iii)), but now $F_v(t)$ is given by Eq (42) (instead of being zero). In this case the gas temperature in the vessel remains almost constant, since substituting the flow rate of Eq (42) into Eq (39) the solution of Eq (43) for $0 < \delta_T < 1$ fulfills that $\lim T(t)_{t\to\infty} = T_0$. In this context, Eq (44) represents the situation in which no cooling-heating flow rate is applied ($F_v(t) = 0$) for $t < t_C$, whereas for $t > t_C$ the applied flow rate is given by Eq (42).

Consequently, the aimed operation of the model corresponds to the previous case iv), i.e., chaotic behavior with an almost constant temperature achieved with the heating-cooling system. The input data and the required parameters for the computational calculations can be summarized as follows:

1) A real gas is considered by specifying its critical constants P_c, T_c, ρ_c, its corresponding ionization potential, polarizability and dipole/quadrupole moments.
2) The input pressure P_1 and the desired pressure P_d in the accumulator vessel are set so that $P_d < P_1$.
3) The input temperatures T_0 for which B and C will be estimated are set.
4) If some input temperature T_0 is below the critical one, the corresponding saturation pressure P_{sat} is calculated by using the Antoine equation given by:

$$\log_{10} P_{sat} = A + \frac{B}{T} + C \log_{10} T + DT + ET^2 \tag{51}$$

and the values of P_1 and P_d are modified so that $P_d < P_1 < P_{sat}$, thus avoiding the biphasic zone of the gas. Although the model can handle pressures and temperatures below the critical ones, in such cases the pressure will be so low that the effect of C or B and C can become negligible in Eq (30).

5) The vessel volume V, the parameters δ, ω_n, K_t, K_d, K_c, τ_I, K_{NLd}, b_0, b_1 and K_m (Eqs (31)-(33)) as well as the servo valve parameters C_f and A_0 (Eq (34)) are set.

Table 5
Variables and parameters used in the Thermodynamic Model

Variable	Description for the Mechanical subsystem	Value
$x_1(t)$	State variable of mechanical subsystem ($mA \cdot s^3$)	
x_{1e}	Equilibrium value of $x_1(t)$ ($mA \cdot s^3$)	
$x_2(t)$	State variable of mechanical subsystem ($mA \cdot s^2$)	
$x_3(t)$	State variable of mechanical subsystem ($mA \cdot s$)	
ω_n	Natural frequency of control valve (rad/s)	0.69
δ	Damping coefficient of control valve	0.26
b_0	Parameter of valve plug position ($1/mA \cdot s^3$)	0.01- 10
b_1	Parameter of the valve plug velocity ($1/mA \cdot s^2$)	$\leq b_0/10$
$x(t)$	Dimensionless valve displacement $b_0x_1(t)+b_1x_2(t)$	
x_e	Equilibrium value of $x(t)$. $x_{1e} = x_e/b_0$	
K_t	Transmitter constant ($16/(2.5 \cdot P_1)$) ($1/N/m^2$)	$3 \cdot 10^{-5}$ to $3.2 \cdot 10^{-6}$
K_{NL}	Constant of nonlinear term ($1/mA^3 \cdot s^6$)	$8 \cdot 10^{-4}$ to 8
τ_I	Integral time of the PI controller (min)	1-900 (300 s)
K_{NL}/τ_I	Defined as $K_{NLd} \cdot f_{KNL}/\tau_I = 8.4146 \cdot 10^{-4} \cdot f_{KNL}/\tau_I$	$1 < f_{KNL} < 10^8$
K_{NLos}	Value of K_{NL} in self-oscillating behavior	$8 \cdot 10^4$ to $8 \cdot 10^8$
C_f	Coefficient of the control valve	0.75
A_0	Area of the gas throughout control valve (m^2)	$4 \cdot 10^{-4}$
ε	Control valve expansion factor	≈ 0.98
K_a	Force constant ($F(t) = K_a \cdot i_{PI}(t)$) (N/mA)	0.3125
$T_m(t)$	Time constant defined as $T_{ma} + AT_m \sin(\omega_{Tm}t)$ (s)	5-10
ω_{Tm}	Frequency for time variation of T_m (rad/s)	0.8
K_m	Parameter defined as $2 \cdot 10^8 P_1/10^5 f_{km}$	$1 < f_{km} < 4$ (2)

Variable	Description for the Thermal subsystem	Value
P_1	Constant line pressure (N/m^2)	$2 \cdot 10^5$ to $8 \cdot 10^6$
P_d	Pressure set point (N/m^2)	$< P_1$
P_{di}	Initial value of P_d for initial conditions (N/m^2)	0.98 to 0.95 of P_d
$P_2(t)$	Pressure in the control valve (State variable) (N/m^2)	$1 \cdot 10^5$ to $7 \cdot 10^6$
$\rho_2(t)$	Inlet gas density (kg/m^3)	1 to 15
T_0	Inlet gas temperature (K)	5-900
$T(t)$	Gas temperature in the vessel (K) (State variable)	5-900
$\rho(t)$	Gas density in the vessel (kg/m^3) (State variable)	0.9 to 14
$P(t)$	Pressure in the vessel (N/m^2) (Calculated with EOS)	$\leq P_2(t)$
V	Volume of the vessel (m^3)	0.001-1 (0.001)
$F_2(t)$	Gas inlet flow rate in CV1 valve (m^3/s)	$5 \cdot 10^{-5}$ to $2.5 \cdot 10^{-4}$
$F_d(t)$	Gas flow rate to the vessel (m^3/s)	$< F_2(t)$
$F_s(t)$	Gas outlet flow rate to the reservoir (m^3/s)	$5 \cdot 10^{-5}$- $2.5 \cdot 10^{-4}$
K_d	Constant of the flow rate $F_d(t)$ $(m^3/s)/(N/m^2)^{0.5}$	$1 \cdot 10^7$
$F_v(t)$	Heating-cooling flow rate in CV2 valve	
ω_{nT}	Natural frequency associated to coil (rad/s)	0.7
δ_T	Damping coefficient associated to heating coil	0.7-0.9
t_C	Time instant at which valve CV2 opens (s)	40-50
$c_p(T)$	Gas heat capacity at constant pressure ($J \cdot kg^{-1} \cdot mol^{-1}$)	
$c_v(T)$	Gas heat capacity at constant volume ($J \cdot kg^{-1} \cdot mol^{-1}$)	

6) An intermolecular potential is set (see Appendix), with which the radial distribution function as a function of the mass density ρ_m given by Eqs (20) and (21) is calculated. In this paper, the parameter values for the considered intermolecular potentials are taken from references [3], [5-11], [15], [23] and [30-32].
7) The pressure, the radial distribution function and the heat capacities are calculated by using Eqs (2), (20), (21) and (25)-(28).
8) The fourth order Runge-Kutta integration method is used to solve numerically the system equations with a simulation step between 0.005 and 0.05 seconds and simulation time of 200 seconds.
9) The chaotic data for the pressure P and specific volume v with an almost constant temperature T in the accumulator vessel are used to estimate $B(T)$ and $C(T)$ by applying the least square method in Eq (30). Such values for $B(T)$ and $C(T)$ estimated from the simulation of the thermodynamic model are compared with the experimental data for $B(T)$ and $C(T)$.
10) An agreement of the values of $B(T)$ and $C(T)$ estimated from chaotic PvT data with the experimental values indicates that the contributions of both $B(T)$ and $C(T)$ are significant in Eq (30) and hence the gas is far from the ideal gas behavior. A discrepancy of the values of $C(T)$ estimated from chaotic PvT data with the experimental values means that $C(T)$ is not significant in Eq (30) for the considered temperature and pressure. And if both $B(T)$ and $C(T)$ estimated from chaotic PvT data are not in agreement with the experimental data then both are not significant in Eq (30) and hence the gas can be regarded as approximately ideal (i.e., compressibility coefficient $z \approx 1$) at the considered pressure and temperature.

The previous steps constitute a general algorithm that can be potentially implemented in a software package using as inputs the gas parameters as well as the intermolecular potential and the desired ranges of pressures and temperatures.

6. Discussion of the results obtained from the thermodynamic model simulation

The procedure described in section 5 will be applied to nitrogen and helium 4.

6.1 Results for nitrogen

The parameter values of the thermodynamic model by using nitrogen taking different input temperatures T_0 are shown in table 6 for the intermolecular potentials considered in the Appendix. It should be noted that the nitrogen is a non-polar gas with quadrupolar moment $\Theta = -5 \cdot 10^{-40}$ C·m^2, i.e. the electric charge distribution of the molecule is approximated by an oblate symmetric top. Consequently, the averaged electrostatic potential given by Eq (A14) is nonzero and the total intermolecular potential depends on the temperature. The equilibrium points x_{1e} of the state variable $x_1(t)$ (Eq (45)) are also shown in table 6 at each input temperature T_0.

Fig 7 a) shows the plot of the RDF given by Eqs (20) and (21) using the Mie potential at three fixed temperatures and densities for which the empirical high precision EOS with 12 parameters of Refs [42], [43] provides a pressure of $8 \cdot 10^6$ N/m^2. Figs 7 b) and c) show the heat capacities at constant volume c_v and pressure c_p calculated using the Mie potential and Eqs (25)-(28) through two different procedures. On one hand, c_{vMie} and c_{pMie} are the respective heat capacities at fixed temperatures and densities for which the general EOS of Eqs (2), (20) and (21) provides a pressure of $8 \cdot 10^6$ N/m^2.

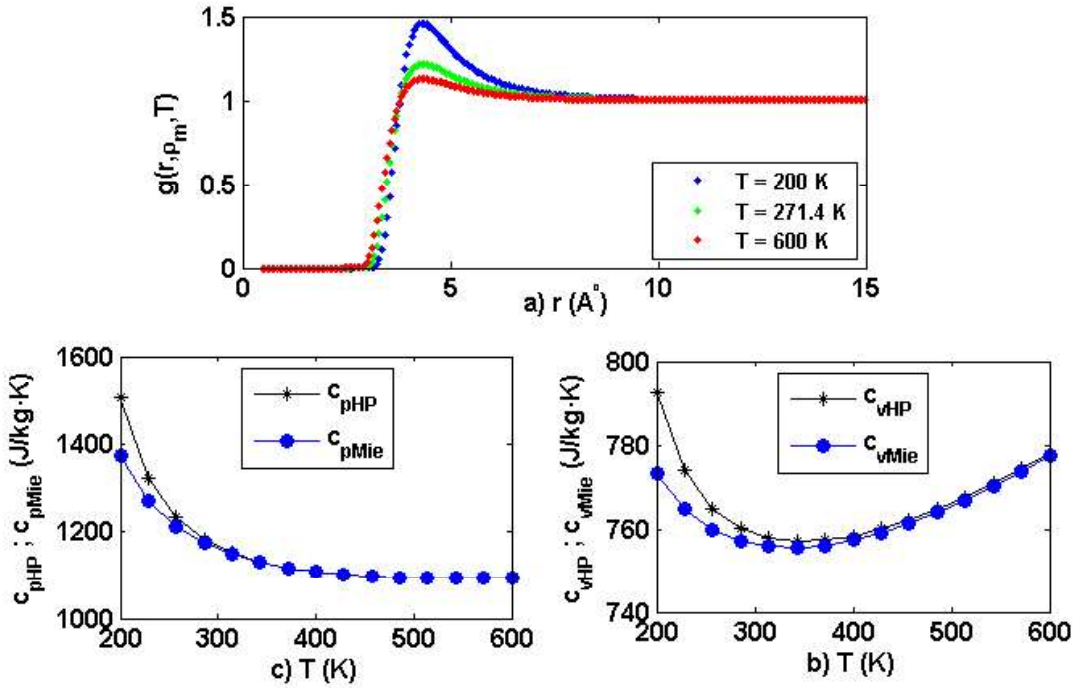

Fig 7. a) Radial distribution function given by Eqs (20) and (21) for N_2 using the Mie potential for a pressure of $8 \cdot 10^6$ N/m^2 and the EOS of Refs [42], [43]. b) Heat capacities at constant volume obtained through Eqs (25)-(28) using the Mie potential for a pressure of $8 \cdot 10^6$ N/m^2 and the EOS of Eqs (2), (20), (21) (c_{vMie}) as well as the EOS of Refs [42], [43] (c_{vHP}). c) Same as figure b) but for the heat capacities at constant pressure (c_{pMie} and c_{pHP}).

On the other hand, c_{vHP} and c_{pHP} are the respective heat capacities at fixed temperatures and densities for which the high precision EOS of Refs [42], [43] provides a pressure of $8 \cdot 10^6$ N/m^2. The heat capacities calculated by both methods are in very good agreement.

Fig 8 shows the PvT chaotic data using the Mie potential for nine different temperatures T_0. Fig 8 a) shows the pressure P_2 at the output of the servo-valve CV1 as well as the choked pressures P_{ch}, whose irregular behavior constitutes a clear indicator of chaotic behavior. In Fig 8 b), the pressure P_2 at the output of the servo-valve CV1 and the pressure P inside the vessel are plotted showing that their values remain very close as a result of an adequate selection of the discharge coefficient K_d of the valve V_2 (see Eq (41)). Figs 8 c) and d) respectively show the densities and the temperatures of the gas inside the vessel.

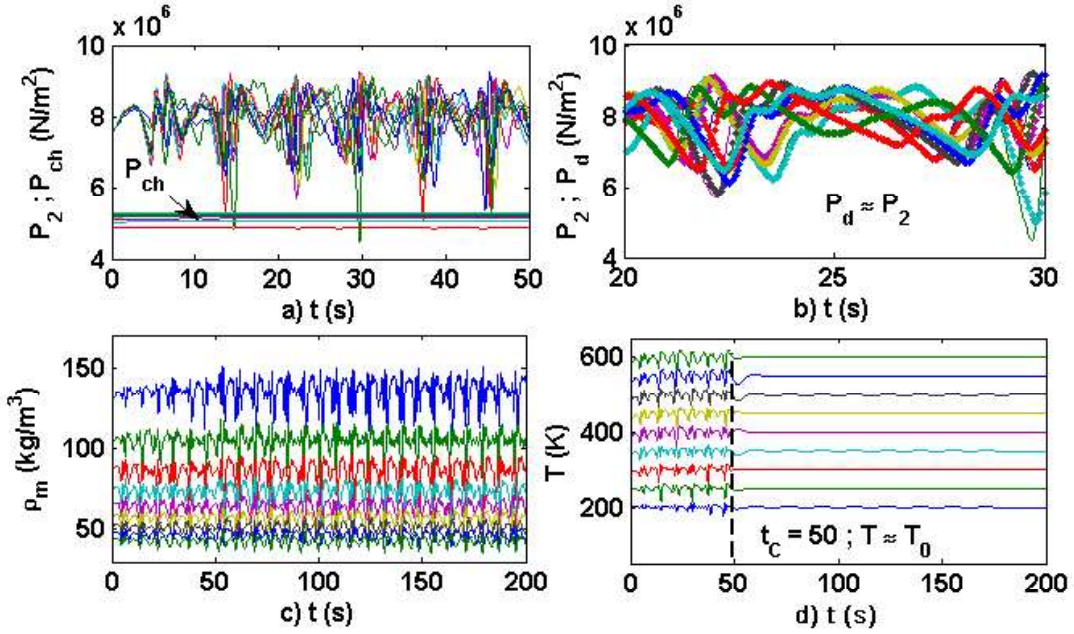

Fig 8. Chaotic behavior for N_2 using the Mie potential for nine input temperatures T_0: 200, 250, 300, 350, 400, 450, 500, 550 and 600 K. a) Chaotic oscillations of the gas pressure P_2 at the output of the valve CV1 and choked pressures P_{ch}. b) Pressure P_2 at the output of the valve CV1 and pressure P inside the vessel for $K_d = 6 \cdot 10^{-7}$. c) Chaotic oscillations of the gas mass density ρ_m inside the vessel for each temperature. d) Temperature chaotic oscillations inside the vessel for $t < t_C = 50$ s and steady-state temperature approximately equal to T_0 for $t \geq t_C$.

It should be noted that the servo-valve CV2 is open for $t > t_C = 50$ s and thus the gas temperature is described by Eqs (44) until it will eventually reach the desired constant temperature T_0. It is interesting to note that the simulation values for the

choked pressures and densities shown in Fig 8 a) are very close to those obtained in the generalized compressibility charts [46], [47].

Table 6
Simulation parameters values and intermolecular potentials for N_2

Parameter values of the mechanical and thermal subsystem. Nomenclature in table 5
$\delta = 0.26$; $\omega_n = 0.69$ rad/s; $K_t = 6.4 \cdot 10^{-7}$ mA·m^2/N; $K_d = 4.8 \cdot 10^{-7}$ (m^3/s)/(N/m^2)$^{0.5}$; $BP = 50$; $K_c = 100/BP$; $\tau_I = 300$ (s); $P_1 = 10^7$ N/m^2; $P_d = 8 \cdot 10^6$ N/m^2 $\omega_{nT} = 0.8$ rad/s; $\delta_T = 0.7$; $V = 1 \cdot 10^{-3}$ m^3; $K_{NLd} = 8.4146 \cdot 10^{-4}$ (1/mA^2·s^6); $K_m = 4.8140 \cdot 10^{10}$ N/m^2
Dipole, quadrupole moments, ionization potential and polarizability
$\mu = 0$; $\Theta = -5 \cdot 10^{-40}$ C·m^2; $I_0 = 2.5314 \cdot 10^{-18}$ J; $\alpha = 1.74 \cdot 10^{-30}$ m^3

Mie Potential (MIE) [2], [3], [4], [8], [15], [36]:
$n = 9$; $\sigma = 3.7980 \cdot 10^{-10}$ m; $\varepsilon = 9.8579 \cdot 10^{-22}$ J
Simulation parameters: $f = 0.5$; $f_{CM} = 10$; $b_0 = 1$ (1/mA·s^3); $b_1 = 0.1$ (1/mA·s^2)

T_0 (K)	200	300	400	500	600
T_{ma} (s)	5	6.25	7.5	8.75	10
AT_m (s)	4.1667	4.6296	5.000	5.3030	5.5556
x_{1e} (mA·s^3)	0.0312	0.0227	0.0224	0.0218	0.0208
K_{NLos} mA^{-2}·s^{-6}	$5.5760 \cdot 10^6$	$4.8852 \cdot 10^6$	$5.5390 \cdot 10^6$	$6.2845 \cdot 10^6$	$7.0576 \cdot 10^6$

Morse potential (MO) [7], [8]
$D = 1.2895 \cdot 10^{-21}$ J; $\alpha = 1.1660 \cdot 10^{10}$ (Å)$^{-1}$; $r_e = 4.43 \cdot 10^{-10}$ Å
Simulation parameters: $f = 0.5$; $f_{CM} = 10$; $b_0 = 1$ (1/mA·s^3); $b_1 = 0.1$ (1/mA·s^2)

T_0 (K)	200	300	400	500	600
T_{ma} (s)	5	6.25	7.5	8.75	10
AT_m (s)	4.1667	4.6296	5.000	5.3030	5.5556
x_{1e} (mA·s^3)	0.0286	0.0264	0.0237	0.0214	0.0195
K_{NLos} mA^{-2}·s^{-6}	$5.3662 \cdot 10^6$	$5.3528 \cdot 10^6$	$5.8715 \cdot 10^6$	$6.5437 \cdot 10^6$	$7.2754 \cdot 10^6$

Kihara potential (KI) [9], [10]
$\varepsilon = 1.9219 \cdot 10^{-21}$ J; $\sigma = 3.5260 \cdot 10^{-10}$ m; $a_K = 7.2219 \cdot 10^{-11}$ m
Simulation parameters: $f = 0.5$; $f_{CM} = 10$; $b_0 = 1$ (1/mA·s^3); $b_1 = 0.1$ (1/mA·s^2)

T_0 (K)	200	300	400	500	600
T_{ma} (s)	5	6.25	7.5	8.75	10
AT_m (s)	4.1667	4.6296	5.000	5.3030	5.5556
x_{1e} (mA·s^3)	0.0286	0.0264	0.0237	0.0214	0.0195
K_{NLos} mA^{-2}·s^{-6}	$5.2488 \cdot 10^6$	$5.3202 \cdot 10^6$	$5.8599 \cdot 10^6$	$6.5288 \cdot 10^6$	$7.2550 \cdot 10^6$

Exp-6 potential (BU) [11], [23]
$P = 1.9409 \cdot 10^{-14}$ J; $\rho = 2.3594 \cdot 10^{-11}$; $\mu_B = 8.9917 \cdot 10^{-78}$ J·m^6
Simulation parameters: $f = 0.5$; $f_{CM} = 8.8$; $b_0 = 1$ (1/mA·s^3); $b_1 = 0.1$ (1/mA·s^2)

T_0 (K)	200	309.09	418.18	527.27	600
T_{ma} (s)	5	6.3636	7.7273	9.0909	10
AT_m (s)	4.1667	4.6667	5.0595	5.3763	5.5556
x_{1e} (mA·s^3)	0.3008	0.2677	0.2351	0.2099	0.1965
K_{NLos} mA^{-2}·s^{-6}	$1.4080 \cdot 10^4$	$1.4790 \cdot 10^4$	$1.6563 \cdot 10^4$	$1.8498 \cdot 10^4$	$1.9798 \cdot 10^4$

Figs 9 a) and b) show the virial coefficients B and C for nitrogen estimated from chaotic pressures and densities with the intermolecular potentials of Mie (MIE), Morse (MO), Kihara (KI) and Buckingham (BU) using the parameters of table 6. Such potentials are used with the general EOS defined by Eqs (2), (20) and (21). In addition, the desired pressure in the accumulator vessel $P_d = 8 \cdot 10^6$ N/m^2 is above the critical one $P_c = 3.439 \cdot 10^6$ N/m^2. The estimations of B and C are accurate for all the potentials at high temperatures, although the MIE and MO potentials lead to better results at low temperatures.

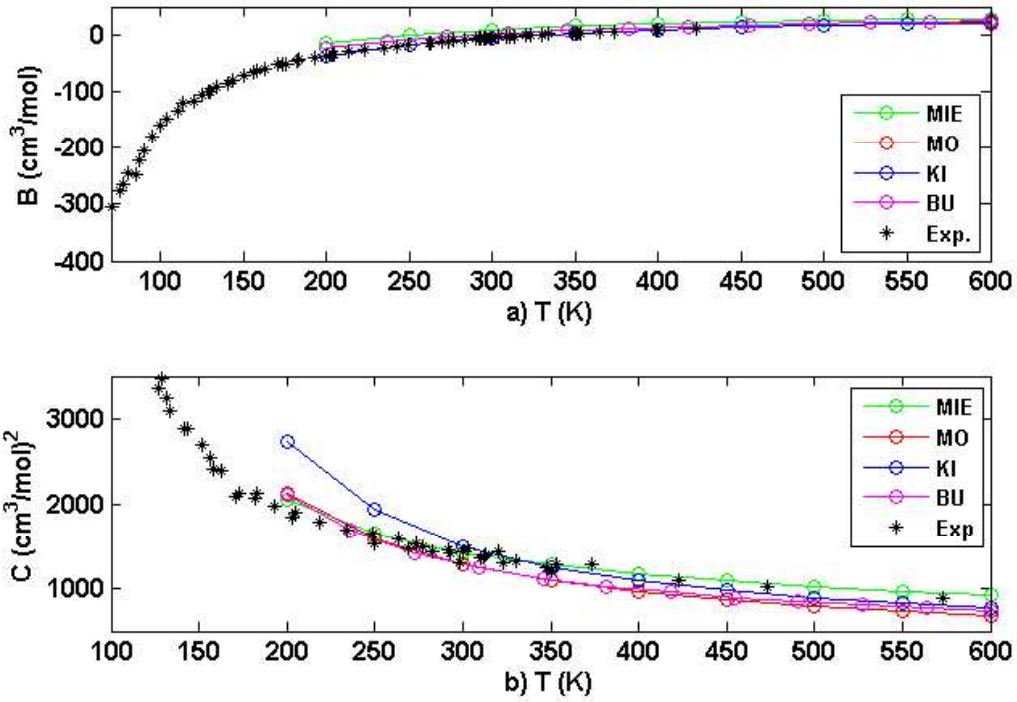

Fig 9. Virial coefficients B (plot a)) and C (plot b)) for N_2 estimated from the chaotic simulated PvT data taking $P_d = 8 \cdot 10^6$ N/m^2 for the intermolecular potentials MIE, MO, KI, BU with the EOS of Eqs (2), (20) and (21). The experimental values (Exp) are marked with asterisks.

The results of figs 8 and 9 have been obtained by simulating the thermodynamic model at nine input temperatures T_0 equally spaced between 200 and 600 K (twelve temperatures have been taken for the Exp-6 potential). However, the experimental values for B and C are available at the temperatures T_{BExp} and T_{CExp} [4] indicated in table 7, at which B and C have also been estimated by simulating the thermodynamic model (which can be done at any temperature) for each intermolecular potential.

Table 7
Values of B and C obtained with the simulation parameters of table 6 for N_2

T_{BExp}, T_{CExp} = Experimental temperatures for B and C from Ref [4]
B_{MIE}, C_{MIE} = Values of B and C obtained with the Mie potential
B_{MO}, C_{MO} = Values of B and C obtained with the Morse potential
B_{KI}, C_{KI} = Values of B and C obtained with the Kihara potential
B_{BU}, C_{BU} = Values of B and C obtained with the Exp-6 (BU) potential
$B_{Exp}\pm\Delta B_{Exp}$ = Experimental values of B from Ref [4]
$C_{Exp}\pm\Delta C_{Exp}$ = Experimental values of C from Ref [4]
DeB(MIE) (%) = Deviation between B_{MIE} and B_{Exp}
DeC(MIE) (%) = Deviation between C_{MIE} and C_{Exp}

$T_0 \equiv T_{BExp}$ K	B_{MIE} cm³/mol	B_{MO} cm³/mol	B_{KI} cm³/mol	B_{BU} cm³/mol	$B_{Exp}\pm\Delta B_{Exp}$ cm³/mol	*DeB*(MIE) %
222.89	-24.434	-26.047	-25.659	-26.121	-24.8±1	1.475
242.00	-18.093	-19.183	-18.838	-19.328	-19.0±2	4.773
262.00	-12.578	-13.262	-12.964	-13.449	-13.0±2	3.246
273.15	-9.897	-10.406	-10.132	-10.606	-9.7±0.5	1.990
289.64	-6.364	-6.659	-6.415	-6.864	-5.9±0.6	7.291
295.00	-5.339	-5.551	-5.317	-5.753	-5.7±1.5	6.333
303.20	-3.791	-3.937	-3.715	-4.139	-4.0±2	5.225
320.00	-0.987	-0.955	-0.740	-1.139	-1.2±0.1	17.750
348.15	3.113	3.285	3.495	3.147	3.2±1	2.718
365.00	5.203	5.450	5.667	5.349	5.2±1.5	5.765
398.15	8.723	9.070	9.319	9.055	9.0±1	3.077
423.15	10.950	11.349	11.637	11.410	11.4±1	3.947

$T_0 \equiv T_{CExp}$ K	C_{MIE} cm⁶/mol²	C_{MO} cm⁶/mol²	C_{KI} cm⁶/mol²	C_{BU} cm⁶/mol²	$C_{Exp}\pm\Delta C_{Exp}$ cm⁶/mol²	*DeC*(MIE) %
234.05	1702.9	1736.4	2037.2	1805.0	1680±200	1.344
263.08	1520.5	1508.0	1739.6	1557.3	1590±200	4.371
276.94	1450.9	1421.4	1630.9	1465.9	1500±200	3.273
293.15	1380.2	1334.0	1524.2	1374.8	1429±75	3.415
310.00	1316.4	1256.0	1430.8	1294.8	1360±100	3.205
320.00	1282.6	1214.8	1382.2	1253.3	1435±50	10.620
330.00	1251.0	1176.3	1338.0	1214.8	1320±100	5.227
348.15	1199.2	1114.0	1267.3	1153.1	1257±50	4.598
350.00	1194.0	1108.1	1260.7	1147.2	1220±100	2.131
373.15	1137.2	1040.7	1185.8	1081.7	1079±50	5.117
423.15	1037.5	924.6	1062.2	970.9	1036±60	1.445
473.15	959.86	836.0	972.9	889.0	1028±30	6.628
573.15	843.58	707.3	852.3	773.9	883±30	4.464

As it can be observed in table 7, the deviations of the values of B and C obtained with the Mie potential are somewhat better than those obtained with other potentials. It

should be noted that the temperatures T_{BExp} and T_{CExp} for the experimental values of B and C do not coincide, so the simulations must be carried out separately for B and C.

6.2 Results for helium 4

Helium 4 is a non-polar gas in which quantum effects for B are especially relevant especially at low temperatures. In this case only the Mie potential will be considered, since both the Morse and Kihara potentials can be assimilated to this one [8], [9], [10], [11] and the Buckingham potential is less utilized. We will focus on the quantum effects and the advantages that can be obtained from the thermodynamic model.

Table 8
Simulation parameter values and Mie potential for He4

Parameters values of the mechanical and thermal subsystem. Nomenclature in table 5
$\delta = 0.26$; $\omega_n = 0.69$ rad/s; $K_t = 8\cdot10^{-7}$ (mA·m^2/N); $K_d = 3.75\cdot10^{-7}$ (m^3/s)/(N/m^2)$^{0.5}$
$C_f = 0.75$; $A_0 = 4\cdot10^{-6}$ m^2; $BP = 50$; $K_c = 100$/BP; $\tau_I = 300$ s; $P_I = 8\cdot10^6$ N/m^2
$P_d = 5.7\cdot10^6$ N/m^2; $\omega_{nT} = 0.8$ rad/s; $\delta_T = 0.7$; $V = 1\cdot10^{-3}$ m^3
Critical Pressure $P_c = 2.28\cdot10^5$ N/m^2
$K_{NLd} = 8.4146\cdot10^{-4}$ (1/mA^2·s^6); $K_m = 3.8512\cdot10^{10}$ N/m^2;
Dipole, quadrupole moments, ionization potential and polarizability
$\mu = 0$; $\Theta = 0$; $I_0 = 3.9573\cdot10^{-18}$ J; $\alpha = 2.00\cdot10^{-29}$ m^3

Mie potential (MI) [3], [4], [6], [15], [36]
$\sigma = 3.7980\cdot10^{-10}$ m; $\varepsilon = 9.8579\cdot10^{-22}$ J; $n = 12.4$
Simulation parameters: $f = 1.3$; $f_{CM} = 13$; $b_0 = 1$ (1/mA·s^3); $b_1 = 0.1$ (1/mA·s^2)

T_0 (K)	80	285.7143	491.4286	697.1429	800
T_{ma} (s)	5	6.0526	7.3684	8.6842	10
AT_m (s)	4.1667	4.5699	5.0000	5.3419	5.5556
x_{1e} (mA·s^3)	0.1747	0.0962	0.0689	0.0565	0.0505
K_{NLos} mA^{-2}·s^{-6}	$0.9230\cdot10^5$	$2.4542\cdot10^5$	$3.9583\cdot10^5$	$5.1308\cdot10^5$	$5.8871\cdot10^5$

The thermodynamic model of Fig 6 has been simulated with the parameters indicated in table 8. Fig 10 shows the heat capacities c_p and c_v calculated through Eqs (2), (20), (21) and (25)-(28) by using the chaotically varying simulated PvT data during 200 s as well as at a constant pressure $P_I = 8\cdot10^6$ N/m^2 as shown in the insets. It can be observed that the values of the heat capacities calculated by both methods are close. Furthermore, the averaged values of c_p and c_v obtained from chaotic PvT data coincide very approximately with the respective values at constant pressure $P_I = 8\cdot10^6$ N/m^2,

which constitutes an indirect verification that the model is consistent with the proposed RDF and EOS.

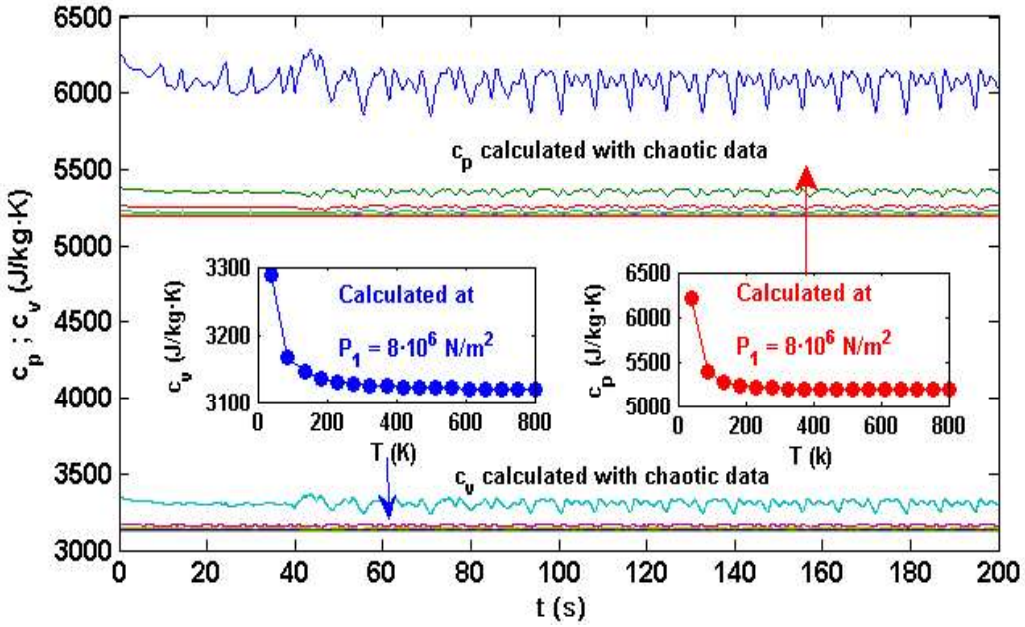

Fig 10. Heat capacities c_p and c_v for He4 calculated through Eqs (2), (20), (21) and (25)-(28) using chaotic PvT data as a function of time t as well as at a constant pressure $P_1 = 8 \cdot 10^6$ N/m^2 in the insets.

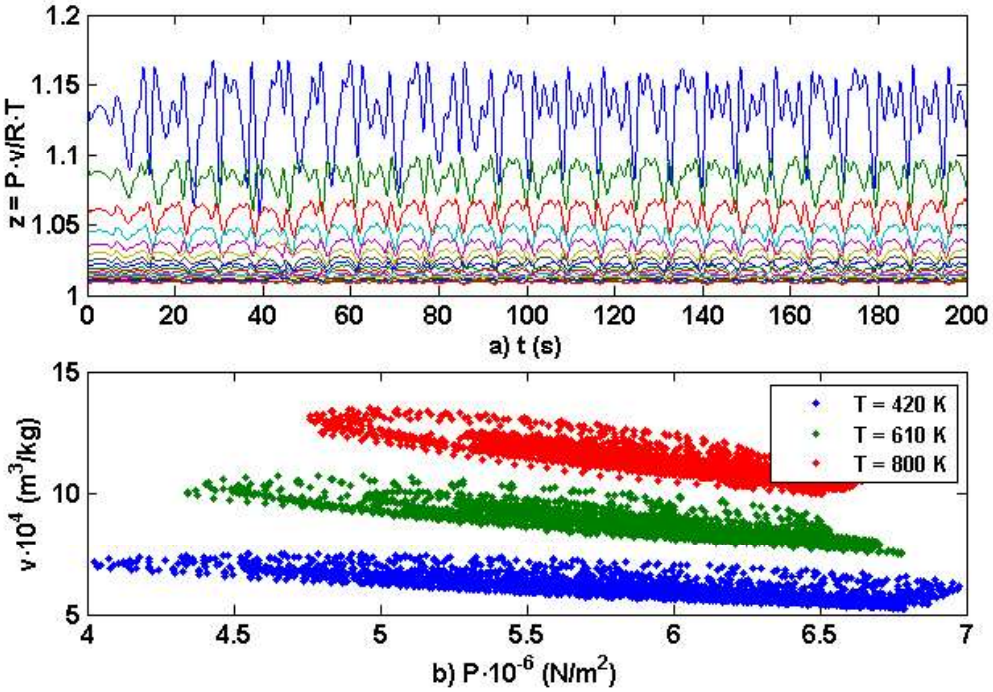

Fig 11. a) Compressibility coefficient z for He4 at seventeen temperatures T_0 as a function of time. b) Three zones of chaotic values in the P-v plane at the temperatures of 420 K, 610 K and 800 K.

Fig 11 a) shows the chaotic variation of the compressibility coefficient z given by Eq (30) as a function of time for each input temperature T_0. Seventeen equally

spaced values for T_0 between 40 and 800 K have been chosen, i.e. 40, 87.5, 135, 182.5, 230, 277.5, 325, 372.5, 420, 467.5, 515, 562.5, 610, 657.5, 705, 752.5 and 800 K. The values of z deviate from unity, so the behavior of He4 is far from that of an ideal gas at the considered pressures and temperatures. Fig 11 b) shows three sets of chaotic data in the P-v plane obtained at the constant temperatures of 420 K, 610 K and 800 K. The chaotic nature of the PvT data is necessary to achieve an accurate estimation of B and C by collecting the gas dynamic properties (if such PvT data had not been chaotic, the estimations of B and C would have been much more inaccurate).

Fig 12 shows the results for the second virial coefficient, where B_{CMie} is the estimation from the chaotic PvT data, B_Q is the quantum correction of Eq (24), B_{Mie} is the calculated value through Eq (22) and the experimental values are marked with asterisks. The simulation is carried out with the values of table 8 applying the heating-cooling flow at t = 40 s and with a desired pressure in the accumulator vessel P_d = $5.7 \cdot 10^6$ N/m^2, which is much above the critical one $P_c = 2.28 \cdot 10^5$ N/m^2. In this case, the estimations B_{CMie} obtained from the chaotic PvT data do not agree with the experimental values, especially at low temperatures at which the quantum effects B_Q are significant as it can be appreciated in the inset of Fig 12. However, the values of $B_{CMie} + B_Q$ are in much better agreement with the experimental data and in turn almost coincident with the values of $B_{Mie} + B_Q$ at all temperatures.

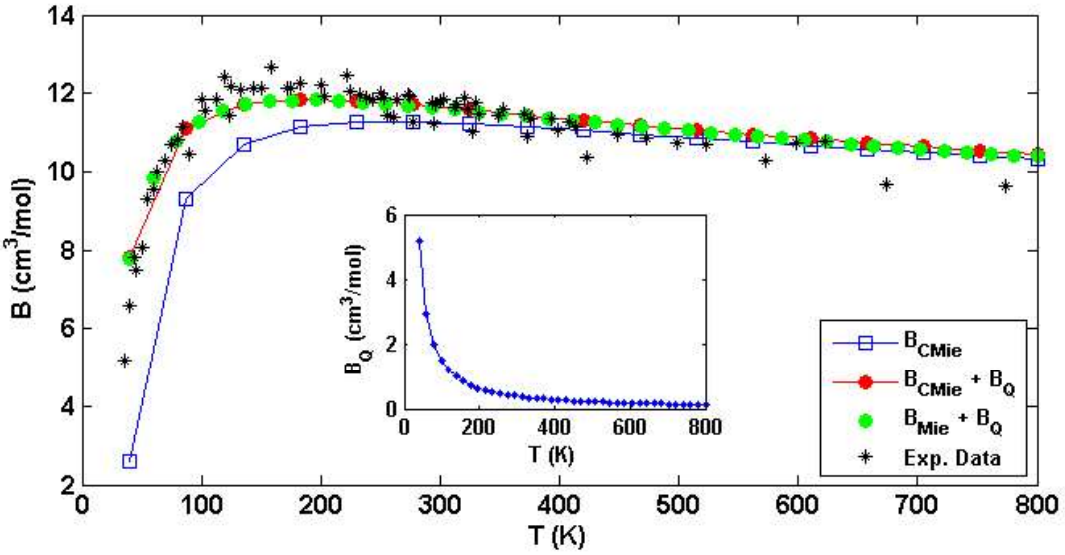

Fig 12. Results for the second virial coefficient for He4 for P_d = $5.7 \cdot 10^6$ N/m^2 (table 8) considering chaotic PvT data (B_{CMie}), quantum effects (B_Q) and the estimation B_{Mie} by using Eq (22).

Table 9 shows the numerical results for $B_{CMie} + B_Q$, $B_{Mie} + B_Q$ for helium4 and their relative deviations respect to the experimental data B_{exp} at their corresponding experimental temperatures T_{BExp} [4]. It can be observed that the deviations are small and that the calculated values are within or near the margin error of the experimental values.

Table 9
Virial coefficients B for He4 with Mie Potential

B_{CMie} = Calculated with chaotic data by using the Mie potential (table 8)
B_{Mie} = Calculated with Mie potential and Eq (20)
B_Q = Quantum correction of B [2], [15]
$B_{Exp} \pm \Delta B_{Exp}$ = Recommended experimental data [4], [48]
T_{BExp} = Experimental temperatures for B [4]
De (%) = Deviation between $B_{CMie} + B_Q$ and B_{Exp}

T_{BExp} K	B_{Mie} cm³/mol	B_{CMie} cm³/mol	B_Q cm³/mol	$B_{CMie}+B_Q$ cm³/mol	$B_{Mie}+B_Q$ cm³/mol	$B_{Exp}\pm\Delta B_{Exp}$ cm³/mol	*De* %
40.09	2.639	2.642	5.169	7.811	7.808	6.57±0.50	15.8
83.80	9.077	9.084	1.861	10.945	10.938	11.13±0.20	1.662
133.15	10.655	10.667	1.032	11.700	11.687	11.97±0.50	2.255
183.15	11.125	11.141	0.698	11.840	11.823	12.09±0.50	2.067
222.13	11.240	11.259	0.553	11.813	11.793	11.93±1.0	0.980
273.15	11.254	11.277	0.433	11.711	11.687	11.80±0.30	0.754
330.00	11.188	11.216	0.347	11.563	11.535	11.75±0.20	1.591
373.55	11.112	11.143	0.300	11.443	11.412	10.90±0.50	4.745
423.25	11.012	11.047	0.259	11.307	11.271	10.36±0.50	8.375
473.15	10.907	10.945	0.228	11.174	11.135	11.07±0.03	0.930
523.20	10.800	10.842	0.203	11.045	11.003	10.69±0.07	3.214
673.15	10.493	10.548	0.152	10.700	10.645	10.45±0.08	2.336
773.15	10.306	10.368	0.130	10.498	10.436	10.26±0.07	2.267

Fig 13 compares the virial coefficient C_{Mie} calculated with Eqs (2), (20), (21) as well as C_{CMie} calculated through the adjustment of chaotic Pv simulated data at constant temperature in Eq (30). For the calculation of C_{CMie}, the data of table 8 are used in two cases: i) For the inlet pressure $P_1 = 8 \cdot 10^6$ N/m^2 and $P_d = 5.7 \cdot 10^6$ N/m^2 at seventeen input temperatures T_0 between 80 K and 800 K; ii) for $P_1 = 12 \cdot 10^6$ N/m^2 and $P_d = 9.5 \cdot 10^6$ N/m^2 at seventeen input temperatures T_0 between 80 K and 800 K. The temperature range is different in each case since at very high pressures the minimum temperature must be increased so that the equilibrium point defined by Eqs (46) is stable.

It is interesting to remark that when the simulation pressure increases the values of C_{CMie} tends to the C_{Mie} values at all temperatures, as it can be observed in Fig 13. This result is in accordance with the idea that a good estimation of C from chaotic PvT data requires high pressures, as it was discussed in point 4) of section 5. On the other hand, the values of C_1 and C_2 (three-molecule interaction and the polarization effect respectively) have been also plotted in Fig 13. As expected, at high temperatures the values of C_1 tend to those of C whereas the polarization effect C_2 tends to zero.

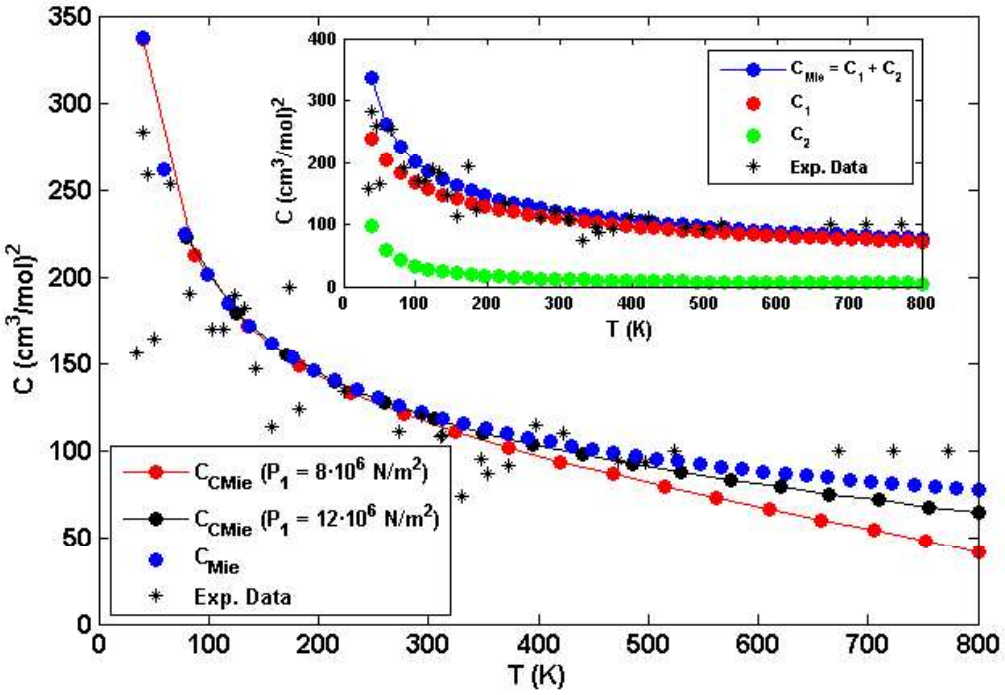

Fig 13. Results for the third virial coefficient for He4. The values of C_1, C_2 and $C_{Mie} = C_1 + C_2$ (inset) are obtained through Eq (22) whereas the values of C_{CMie} are obtained through the chaotic PvT simulated data for two input pressures in the thermodynamic model: $P_1 = 8 \cdot 10^6$ N/m^2 ($P_d = 5.7 \cdot 10^6$ N/m^2) and $P_1 = 12 \cdot 10^6$ N/m^2 ($P_d = 9.5 \cdot 10^6$ N/m^2).

Figs 14 a) and b) show the estimations $B_{CMie} + B_Q$ and C_{CMie} of the second and third virial coefficients respectively for He4 at seventeen temperatures setting $P_d = 2.45 \cdot 10^5$ N/m^2, which unlike in the previous cases is slightly above the critical pressure $P_c = 2.28 \cdot 10^5$ N/m^2. In this case, the estimations of B and C do not fit the experimental data because B and C have little contribution in the virial equation (30) with such a low pressure P_d, i.e. He4 behaves approximately as an ideal gas with $z \approx 1$. Hence the estimation of B and C through the chaotic PvT data is not accurate for very low

pressures at which the gas behavior is nearly ideal and B and C are not significant in Eq (30). Consequently, whilst Eq (22) allows to calculate B and C for any intermolecular potential regardless the pressure, the estimation from chaotic PvT data allows to elucidate if the coefficients B and C are significant in Eq (30) for a considered range of pressures and temperatures.

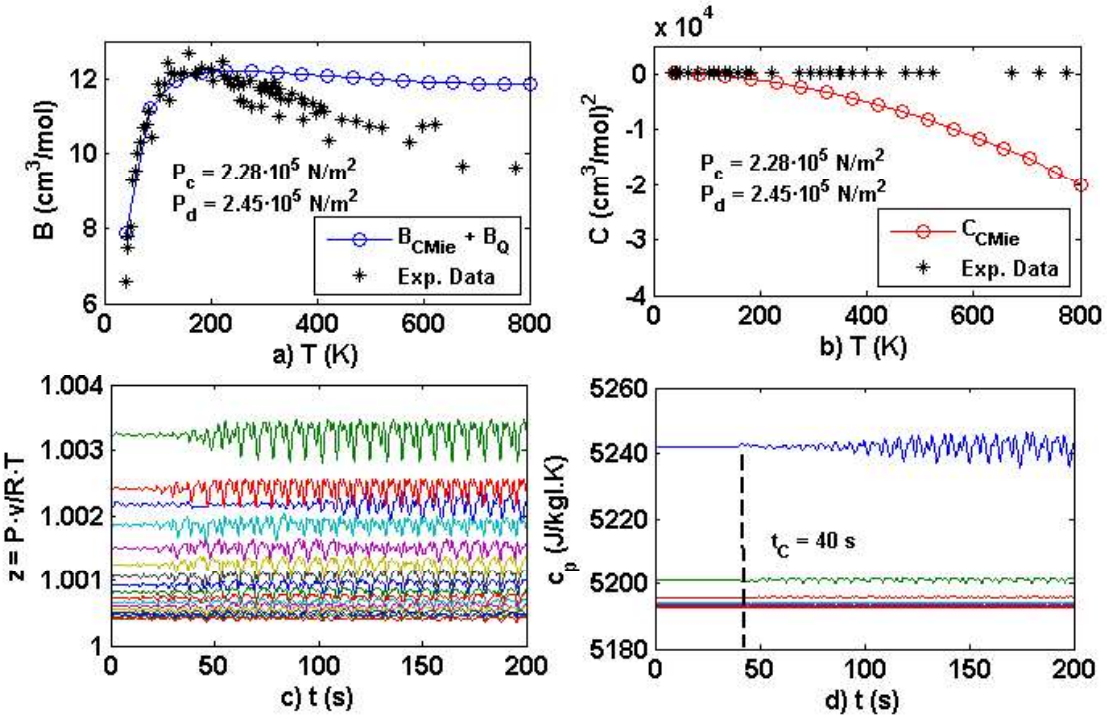

Fig 14. Results for the virial coefficients for He4 with $P_d = 2.45 \cdot 10^5$ N/m^2. a) Estimation $B_{CMie} + B_Q$ of the second virial coefficient from chaotic PvT data including quantum effects. b) Estimation C_{CMie} of the third virial coefficient from chaotic PvT data. c) Compressibility factor z as a function of time t for the temperatures at which B and C are shown in plots a) and b). c) Heat capacity c_p at constant pressure as a function of time t obtained from chaotic PvT data.

Fig 14 c) shows the compressibility coefficient z as a function of time for each of the seventeen temperatures at which $B(T)$ and $C(T)$ have been estimated in plots a) and b). As expected, z oscillates chaotically with values that are very close to unity, that is, He4 behaves approximately as an ideal gas. Fig 14 d) shows the heat capacity c_p as a function of time for each temperature at which $B(T)$ and $C(T)$ have been estimated. It is observed that the oscillation remains chaotic even though at the instant $t = t_c = 40$ s the heating-cooling flow rate $F_v(t)$ has been applied to stabilize the temperature. It should be remarked that the proposed methodology allows determining heat capacities, densities, and compressibility coefficients for a given intermolecular potential in a very wide range of pressures and temperatures.

Table 10 shows the numerical results of C for He4 at the temperatures T_{CExp} at which the experimental values for C are available [4] including the calculation of C_{Mie} through Eq (22) (as it was done in section 3 for Ne and water steam).

Table 10
Virial coefficient C for He4 with Mie Potential

C_{Mie} = Calculated with Mie potential and Eq (20)
C_{CMie} = Calculated with chaotic data by using the Mie potential (table 8) at different input pressures: $P_1 = 3\cdot10^5$ N/m^2 ; $P_1 = 8\cdot10^6$ N/m^2 ; $P_1 = 12\cdot10^6$ N/m^2 and desired pressures in the vessel: $P_d = 2.5\cdot10^5$ N/m^2 ; $P_d = 6\cdot10^6$ N/m^2 ; $P_d = 10\cdot10^6$ N/m^2
$C_{Exp}\pm\Delta C_{Exp}$ = Recommended experimental data [4], [48]
T_{CExp} = Experimental temperatures for C [4]
De (%) = Deviation between C_{CMie} at $P_d = 10\cdot10^6$ N/m^2 and C_{Exp}
$P_c = 2.28\cdot10^5$ N/m^2 < P_d; $\alpha = 2\cdot10^{-31}$ m^3; $I_0 = 3.9574\cdot10^{-18}$ J; $f = 1.3$; $f_{CM} = 13$

T_{CExp} **K**	C_{Mie} **cm^6/mol^2**	C_{CMie} **cm^6/mol^2 $P_d = 2.5\cdot10^5$ N/m^2**	C_{CMie} **cm^6/mol^2 $P_d = 6\cdot10^6$ N/m^2**	C_{CMie} **cm^6/mol^2 $P_d = 10\cdot10^6$ N/m^2**	$C_{Exp}\pm\Delta C_{Exp}$ **cm^6/mol^2**	***De*** **%**
83.15	223.091	-11.79	218.27	218.56	190±10	13.06
133.15	178.102	-405.30	173.21	173.99	182±10	4.40
183.15	153.835	-919.68	148.53	149.97	150±10	0.02
223.15	140.641	-1435.0	134.72	136.74	134±4	2.00
273.15	128.302	-2303.1	121.38	124.20	130±30	4.46
330.00	117.758	-3547.9	109.06	113.35	74±100	34.71
373.15	111.365	-4562.4	101.35	106.32	115±6	7.54
423.15	105.171	-5535.5	92.81	99.44	100±10	0.56
473.15	99.948	-6959.7	85.01	93.27	94±7	0.77
523.15	95.463	-8508.8	77.91	87.84	100±10	12.16
673.15	85.035	-14853	57.37	74.14	100±10	25.86
773.15	79.776	-19683	44.32	65.77	100±10	34.23

In table 10, it is interesting to note that at very low pressures ($P_d = 2.5\cdot10^5$ N/m^2) the estimation of C is very bad since He4 behaves as an almost ideal gas and thus C does not influence in Eq (30) (the same occurs with B as shown in fig 14 a)). As the pressure in the accumulator vessel is increased ($P_d = 6\cdot10^5$ N/m^2 and $P_d = 10\cdot10^5$ N/m^2) the estimation of C improves. Nonetheless, it should be noted that the pressure increase will be limited for physical reasons and numerical limitations in the thermodynamic model simulation. The last column of table 10 shows the relative deviations between the values of C_{CMie} calculated for $P_d = 10\cdot10^5$ N/m^2 and the experimental values C_{Exp}, which can be regarded as admissible given the large variability of experimental data for C.

7 Conclusions

A new general equation of state (EOS) that can be used with any real gas and intermolecular potential has been derived through an approximation of the radial distribution function (RDF) based on the Ornstein-Zernike equation. Such general EOS has been applied to estimate the virial coefficients B and C using two approaches. On one hand, B and C have been directly computed from the proposed EOS for neon and water steam considering the Mie potential and including quantum corrections for Ne as well as dipole-dipole interactions in the Mie potential for water steam. On the other hand, the general EOS has been applied in the context of a thermodynamic model to estimate B and C for nitrogen and helium 4 by adjusting the chaotic Pv data at an almost constant temperature and comparing the estimated values with the experimental ones.

The thermodynamic model includes two servo-valves, a pressure probe, piping connections, a coil of heating-cooling an accumulator vessel and two controllers to regulate the flow rate and temperature. This model has been applied by considering the Mie, Morse, Kihara and Buckingham potentials, including the quantum correction for B in the case of He4 and the quadrupole moments in the Mie potential for nitrogen.

The direct calculation of B and C from the proposed EOS using the Mie potential has allowed to obtain values of B and C in very good agreement with the experimental data for Ne and water steam. In addition, it has been corroborated that the calculations of B are in very good agreement with its general analytical expression for Ne in the absence of dipolar interactions, which however must be considered for water steam.

On the other hand, the estimations of B and C for nitrogen and helium 4 from the chaotic PvT data obtained through the thermodynamic model agree with the experimental data in wide ranges of pressures and temperatures. However, it has been demonstrated that the estimations of B and C through chaotic PvT data are not accurate for very low pressures at which the gas behavior is approximately ideal and hence B and C are not significant in the virial equation. Consequently, the estimation of B and C by using chaotic PvT data allows elucidating if the coefficients B and C are significant in the virial equation for a considered range of pressures and temperatures.

The advantages of the virial coefficient estimation from chaotic PvT data can be summarized as follows. Firstly, it can be used with any intermolecular potentials including dipole and/or quadrupole moments as well as quantum effects. Secondly, it allows to know the pressure and temperature ranges for which both virial coefficients B and C are significant in the virial equation. Thirdly, it can be easily extended to analyze the intermolecular potentials in gas mixtures. And finally, it can be applied for any real gas, thus allowing to determine heat capacities, densities, and compressibility coefficients without the need of resorting to empirical equations of state.

A Appendix

A.1 Intermolecular potentials for non-polar gases.

i) The Mie's intermolecular potential (MI) is defined as [2]:

$$u(r) = \frac{\varepsilon\left(n^n/m^m\right)^{1/(n-m)}}{n-m}\left[\left(\frac{\sigma}{r}\right)^n - \left(\frac{\sigma}{r}\right)^m\right] \tag{A1}$$

where n and m are positive constants with $n > m$, r is the separation between centers of molecules, σ and ε are parameters which depend of the gas considered. Eq (A1) has a minimum u_{min} at a certain distance r_{min}, where $\varepsilon = -u_{min}$ and σ is the intermolecular separation when $u = 0$. The value $n = 12$ is widely accepted for analytical calculations [1], [3], [8], [34], [36] which leads to the Lennard-Jones potential (LJ) given by:

$$u(r) = 4\varepsilon\left[\left(\frac{\sigma}{r}\right)^{12} - \left(\frac{\sigma}{r}\right)^6\right] \tag{A2}$$

ii) The Morse potential (MO) has the advantage that its parameters can be either estimated from experimental data for the second virial coefficient or deduced from the Lennard-Jones potential. In addition, many problems in Quantum Mechanics can be solved analytically by using the MO potential [7], [44], [45], which is defined as:

$$u(r) = D\left\{\exp\left[-2\alpha\left(r - r_e\right)\right] - 2\exp\left[-\alpha\left(r - r_e\right)\right]\right\} \tag{A3}$$

The potentials *u(r)* given in Eqs (A2) and (A3) can be regarded as equivalent when the parameters *D,* α and r_e are given by [8], [44], [45]:

$$r_e = 4^{1/12}\sigma \;\; ; \;\; \alpha = \frac{\ln(2)}{\sigma\left(4^{1/12} - 1\right)} \;\; ; \;\; D = \varepsilon \tag{A4}$$

v) Kihara potential (KI) [9], [10]. Whereas the Lennard-Jones potential assumes that electronic clouds are soft and therefore penetrable (thus allowing molecule overlapping), the Kihara potential assumes a hard core with a soft electronic cloud and it is defined as:

$$u(r) = \begin{cases} \infty \text{ for } r < 2a_K \\ 4\varepsilon\left[\left(\dfrac{\sigma - 2a_K}{r - 2a_K}\right)^{12} - \left(\dfrac{\sigma - 2a_K}{r - 2a_K}\right)^{6}\right] \text{ for } r > 2a_K \end{cases} \tag{A5}$$

where a_K is the radius of the hard core.

vi) Buckingham (BU) –or the Exp(6)- potential. This potential can be considered as an extension of the Sutherland potential substituting the hard core by an exponential term, which leads to [11]:

$$u(r) = Pe^{-r/\rho} - \frac{\mu}{r^6} \tag{A6}$$

where *P*, ρ and μ are parameters which were originally estimated for He4, Ne and Ar [28,29]. Eq (A6) will be used in the form:

$$u(r) = \frac{\alpha\varepsilon}{\alpha - 6}\left[\frac{6e^{\alpha}}{\alpha}e^{-\alpha r/r_m} - \left(\frac{r_m}{r}\right)^6\right] \tag{A7}$$

where α is the slope of the exponential term and ε is the minimum of the potential energy. From Eqs (A6) and (A7) it is follows that:

$$P = \frac{6\varepsilon e^{\alpha}}{\alpha - 6} \;\; ; \;\; \rho = \frac{r_m}{\alpha} \;\; ; \;\; \mu = \frac{\varepsilon e^{\alpha}}{\alpha - 6} r_m^6 \tag{A8}$$

Eqs (A8) will be used to calculate the values of P, ρ and μ from the experimental values of ε, α and r_m [11-23].

A.2 Intermolecular potentials for polar gases.

For molecules with a permanent dipolar moment, the Stockmayer potential consists of the Lennard-Jones potential plus a term that accounts for the potential energy due to dipole-dipole, dipole-quadrupole and quadrupole-quadrupole interactions [5]. In this case, the potential energy $u(r,T)$ depends on the intermolecular distance r and on the temperature T due to the molecular orientation, i.e.:

$$u(r,T) = u_{LJ} + \overline{u}_e(r,\theta_1,\theta_2,\phi_1-\phi_2) = 4\varepsilon\left[\left(\frac{\sigma}{r}\right)^{12} - \left(\frac{\sigma}{r}\right)^{6}\right] + \overline{u}_e(r,\theta_1,\theta_2,\phi_1-\phi_2) \tag{A9}$$

where $\overline{u}_e$ is an averaged electrostatic potential that depends on the dipole orientation angles θ_1, θ_2 and the angles ϕ_1, ϕ_2 which define the relative spin of the dipoles with respect to the axis passing through their centers. The values of the non-averaged potential u_e for pure gases in SI units is given by:

$$u_e \equiv \begin{cases} u_{\mu\mu}(r) = -\dfrac{\mu^2}{4\pi\varepsilon_0 r^3}\left[2\cos\theta_1\cos\theta_2 - \sin\theta_1\sin\theta_2\cos(\phi_1-\phi_2)\right] \\ u_{\mu\Theta}(r) = \dfrac{3\mu\Theta}{8\pi\varepsilon_0 r^4}\left\{(\cos\theta_2 - \cos\theta_1)\left[\begin{array}{c} 3\cos\theta_1\cos\theta_2 - 2\sin\theta_1\sin\theta_2\cos(\phi_1-\phi_2) \\ -(\cos\theta_1 - \cos\theta_2) \end{array}\right]\right\} \\ u_{\Theta\Theta}(r) = \dfrac{3\Theta^2}{16\pi\varepsilon_0 r^5}\left\{\begin{array}{l} 1 - 5\cos^2\theta_1 - 5\cos^2\theta_2 - 15\cos^2\theta_1\cos^2\theta_2 \\ +2\left[\sin\theta_1\sin\theta_2\cos(\phi_1-\phi_2) - 4\cos\theta_1\cos\theta_2\right]^2 \end{array}\right\} \end{cases}$$

(A10)

where $u_{\mu\mu}$, $u_{\mu\Theta}$ and $u_{\Theta\Theta}$ are the dipole-dipole, dipole-quadrupole and quadrupole-quadrupole interaction potentials, μ and Θ are the dipolar and quadrupolar moments and ε_0 is the vacuum dielectric constant. The potentials must be averaged for all possible orientations [2], i.e.:

$$\overline{u}_e = -kT \ln \frac{\int e^{-u_e/kT} \mathrm{d}\Omega}{\int \mathrm{d}\Omega} \quad ; \quad \mathrm{d}\Omega = \sin\theta_1 \sin\theta_2 \mathrm{d}\theta_1 \mathrm{d}\theta_2 \mathrm{d}\phi \quad ; \quad \phi = \phi_1 - \phi_2 \tag{A11}$$

where dΩ is a differential solid angle, $0 \le \theta_1 \le \pi$, $0 \le \theta_2 \le \pi$, $0 \le \phi \le 2\pi$ and therefore $\int \mathrm{d}\Omega = 8\pi$. Considering the dipole-dipole interaction, denoting by $a = \mu^2 / 4\pi\varepsilon_0 r^3$ and expanding the exponential of Eq (A11) it is deduced that:

$$\overline{u}_{\mu\mu} = -kT \ln \frac{\int e^{-u_e/kT} \mathrm{d}\Omega}{\int \mathrm{d}\Omega} = -kT \ln \left[1 + \frac{1}{3} \frac{a^2}{k^2 T^2} + \frac{3}{75} \frac{a^4}{k^4 T^4} + \frac{1421}{540225} \frac{a^6}{k^6 T^6} + ... \right] \tag{A12}$$

Since $\ln(1+x) \approx x - x^2/2 + x^3/3 - ...$, Eq (A12) can be approximated as:

$$\overline{u}_{\mu\mu} \approx -\frac{1}{3} \frac{\mu^4}{(4\pi\varepsilon_0)^2 r^6} \frac{1}{kT} + \frac{7}{450} \frac{\mu^8}{(4\pi\varepsilon_0)^4 r^{12}} \frac{1}{k^3 T^3} \tag{A13}$$

Similarly, the dipole-quadrupole and quadrupole-quadrupole interactions can be approximated up to the first term as:

$$\overline{u}_{\mu\Theta} \approx -\frac{1}{2} \frac{\mu^2 \Theta^2}{(4\pi\varepsilon_0)^2 r^8} \frac{1}{kT} \quad ; \quad \overline{u}_{\Theta\Theta} \approx -\frac{7}{5} \frac{\Theta^4}{(4\pi\varepsilon_0)^2 r^{10}} \frac{1}{kT} \tag{A14}$$

As per Eqs (A10)-(A13), the total averaged electrostatic potential can be approximated as:

$$\overline{u}_e \approx -\frac{1}{3} \frac{\mu^4}{(4\pi\varepsilon_0)^2 r^6} \frac{1}{kT} - \frac{1}{2} \frac{\mu^2 \Theta^2}{(4\pi\varepsilon_0)^2 r^8} \frac{1}{kT} - \frac{7}{5} \frac{\Theta^4}{(4\pi\varepsilon_0)^2 r^{10}} \frac{1}{kT} + \frac{7}{450} \frac{\mu^8}{(4\pi\varepsilon_0)^4 r^{12}} \frac{1}{k^3 T^3} \tag{A15}$$

It should be noted that the Lennard-Jones potential in Eq (A9) may be substituted by the MO, KI or the BU potentials to investigate their effect in the calculation of virial coefficients of a given gas. Values of the dipole moments for different gases can be found in Refs [24], [25].

References

[1] J. E. Jones, On the Determination of Molecular Fields.–II. From the Equation of State of a Gas, Proc. R. Soc. Lond. A **106** (1924) 463–477. https://doi.org/10.1098/rspa.1924.0082

[2] J.P.M. Trusler, The virial equation of state, in: J.V. Sengers, R.F. Kayser, C.J. Peters, H., J. White, Jr. (Eds), Equations of State for Fluids and Fluid Mixtures, IUPAC Commission on Thermodynamics, Elsevier, Amsterdam, 2000, pp. 35–74. https://doi.org/10.1016/S1874-5644(00)80014-4

[3] P. Vargas, E. Muñoz, L. Rodríguez, Second virial coefficient for the Lennard–Jones potential, Physica A **290** (2001) 92–100. https://doi.org/10.1016/S0378-4371(00)00362-9

[4] J.D. Dymond, K.N. Marsh, R.C. Wilhoit, Virial Coefficients of Pure Gases and Mixtures, Springer Verlag, Berlin, 2002.

[5] W.H. Stockmayer, Second Virial Coefficients of Polar Gases, J. Chem. Phys. **9** (1941) 398–402. https://doi.org/10.1063/1.1750922

[6] F.M. Mourits, F.H.A. Rummens, A critical evaluation of Lennard-Jones and Stockmayer potential parameters and of some correlation methods, Can. J. Chem. **55** (1977) 3007–3020. https://doi.org/10.1139/v77-418

[7] P. Morse, Diatomic Molecules According to the Wave Mechanics. II. Vibrational Levels, Phys. Rev. **34** (1929) 57–64. https://doi.org/10.1103/PhysRev.34.57

[8] T.-C. Lim, The Relationship between Lennard-Jones (12-6) and Morse Potential Functions, Z. Naturforsch. **58a** (2003) 615–617. https://doi.org/10.1515/zna-2003-1104

[9] T. Kihara, Determination of Intermolecular Forces from the Equation of State of Gases. J. Phys. Soc. Jpn. **3** (1948) 265–268. https://doi.org/10.1143/JPSJ.3.265

[10] T. Kihara, Virial Coefficients and Models of Molecules in Gases. B, Rev. Mod. Phys. **27** (1955) 412–423. https://doi.org/10.1103/RevModPhys.27.412

[11] R.A. Buckingham, The classical equation of state of gaseous helium, neon and argon, Proc. R. Soc. Lond. A **168** (1938) 264–283. https://doi.org/10.1098/rspa.1938.0173

[12] H.W. Graben, R.D. Present, Evidence for Three-Body forces from Third Virial Coefficients, Phys. Rev. Lett. **9** (1962) 247–248. https://doi.org/10.1103/PhysRevLett.9.247

[13] J.L. Yarnell, M.J. Katz, R.G. Wenzel, S.H. Koenig, Structure Factor and Radial Distribution Function for Liquid Argon at 85 °K, Phys. Rev. A **7** (1973) 2130–2144. https://doi.org/10.1103/PhysRevA.7.2130

[14] T.L. Hill, Statistical Mechanics: Principles and Selected Applications. Dover, New York, 2003.

[15] L.E. Reichl, A Modern Course in Statistical Physics, second ed., John Wiley & Sons, New York, 1988.

[16] M.F. Pérez-Polo, M. Pérez-Molina, E. Fernández-Varó, J. Gil-Chica, Estimation of the virial coefficients by means of chaotic oscillations of pressure and density: Application to quantum gases with cubic equations of state, Fluid Phase Equilib. **473** (2018) 262–285. https://doi.org/10.1016/j.fluid.2018.06.015

[dataset] [17] Emerson Process Management, Control Valve Handbook. fourth ed. https://www.emerson.com/documents/automation/control-valve-handbook-en-3661206.pdf

[dataset] [18] Metso Automatic Inc, Flow control manual. Vanha Porvoontie, sixth ed. Finland. http://valveproducts.metso.com/documents/softwarepackages/nelprof/FlowControl_manual.pdf, 2011.

[dataset] [19] Design instrument series BS-2100, BS-2200, BS-2300, BS-2400, BS-2500, http://www.electroson.com/documentos/D_BS2500LLC_0_DESIN_BS2500_PDF.pdf, 2015

[20] J.W. Hutchinson, ISA Handbook of Control Valves, second ed., Instrument Society of America. Research Triangle Park, D.C., U.S.A, 1976.

[21] K. Ogata, Systems Dynamics, first ed., Prentice Hall, New York, 1980.

[22] V.M. Bannur, Virial expansion and condensation with a new generating function, Physica A **419** (2015) 675–680. https://doi.org/10.1016/j.physa.2014.10.053

[23] B.A. Mamedov, E. Somuncu, Accurate calculation of second virial coefficient of the Exp-6 potential and its application, Physica A **420** (2015) 246–257. https://doi.org/10.1016/j.physa.2014.11.014

[24] L.G. MacDowell, C. Menduiña, C. Vega, E. de Miguel, Third virial coefficients and critical properties of quadrupolar two center Lennard-Jones models, Phys. Chem. Chem. Phys. **5** (2003) 2851–2857. https://doi.org/10.1039/b302780e

[25] Y.V. Kalyuzhnyi, I.A. Protsykevitch, P.T. Cummings, Liquid-gas phase behavior of Stockmayer fluid with high dipolar moment, Con. Matter Phys. **52** (2007) 553–562. https://doi.org/10.5488/CMP.10.4.553

[26] B.M. Axilrod, E. Teller, Interaction of the van der Waals Type Between Three Atoms, J. Chem. Phys. **11** (1943) 299-300. https://doi.org/10.1063/1.1723844

[27] Y. Muto, Force between nonpolar molecules, J. Phys.-Math. Soc. Jpn. **17** (1943) 629–631. https://doi.org/10.11429/subutsukaishi1927.17.10-11-12_629

[28] A. Kumar, A.J. Thakkar, 2010. Dipole oscillator strength distributions with improved high-energy behavior: Dipole sum rules and dispersion coefficients for Ne, Ar, Kr, and Xe revisited, J. Chem. Phys. **132**, 074301. https://doi.org/10.1063/1.3315418

[29] G. Marcelli, R.J. Sadus, Molecular simulation of the phase behavior of noble gases using accurate two-body and three-body intermolecular potentials, J. Chem. Phys. **111** (1999) 1533-1540. https://doi.org/10.1063/1.479412

[30] M. Vlasiuk, R.J. Sadus, 2017. Predicting vapor-liquid phase equilibria with augmented *ab initio* interatomic potentials, J. Chem. Phys. **146**, 244054. https://doi.org/10.1063/1.4986917

[31] J.A. Barker, D. Henderson, Perturbation Theory and Equation of State for Fluids. II. A Successful Theory of Liquids, J. Chem. Phys. **47** (1967) 4714–4721. https://doi.org/10.1063/1.1701689

[32] J.A. Barker, D. Henderson, What is "liquid"? Understanding the states of matter, Rev. Mod. Phys. **48** (1976) 587-671. https://doi.org/10.1103/RevModPhys.48.587

[33] C.L. Yaws, Chemical Properties Handbook, McGraw-Hill, New York, 1999.

[34] R.J. Sadus, 2018. Second virial coefficient properties of the *n-m* Lennard-Jones/Mie potential, J. Chem. Phys. **149**, 074504. https://doi.org/10.1063/1.5041320
[35] R.J. Sadus, 2019. Erratum: "Second virial coefficient properties of the *n-m* Lennard-Jones/Mie potential" [J. Chem. Phys. 149, 074504 (2018)], J. Chem. Phys. **150**, 079902. https://doi.org/10.1063/1.5091043
[36] J.R. Mick, M.S. Barhaghi, B. Jackman, K. Rushaidat, L. Schwiebert, J.J. Potoff, 2015. Optimized Mie potentials for phase equilibria: Application to noble gases and their mixtures with n-alkanes, J. Chem. Phys. **143**, 114504. https://doi.org/10.1063/1.4930138
[37] R.A. Svehla, Estimated Viscosities and Thermal Conductivities of Gases at High Temperatures, NASA Tech. Report R-132. Lewis Research Center, Cleveland, Ohio (1962).
[38] W. Wagner, H.-J. Kretzschmar, International Steam Tables. Properties of Water and Steam Based on the Industrial Formulation IAPWS-IF97, second ed., Springer, 1997.
[39] L.P. Shilnikov, A.L. Shilnikov, D.V. Turaev, L.O. Chua. Methods of Qualitative Theory in Nonlinear Dynamics. Part II, World Scientific, New Jersey, 2001.
[40] J. Guckenheimer, P.J. Holmes, Nonlinear Oscillations, Dynamical Systems, and Bifurcations of Vector Fields, Springer, New York, 1983.
[41] S. Wiggins, Introduction to Applied Nonlinear Dynamical Systems and Chaos, second, Springer, New York, 2000.
[42] E.W. Lemmon, R. Span, Multi-parameter Equations of State for Pure Fluids and Mixtures, in: A.R.H. Goodwin, J.V. Sengers, C.J. Peters (Eds), Applied Thermodynamics of Fluids, IUPAC, Physical and BioPhysical Chemistry Division, RSC Publishing, Cambridge, 2010, pp. 394–432.
[43] R. Span, W. Wagner, Equations of State for Technical Applications. I. Simultaneously Optimized Functional Forms for Nonpolar and Polar Fluids, Int. J. Thermophys. **24** (2003) 1–39. https://doi.org/10.1023/A:1022390430888
[44] A. Matsumoto, Parameters of the Morse Potential from Second Virial Coefficients of Gases, Z. Naturforsch. **42a** (1987) 447–450. https://doi.org/10.1515/zna-1987-0505
[45] A. Matsumoto, Takahasi Nearest-Neighbour Gas Revisited II: Morse Gases, Z. Naturforsch. **66a** (2011) 774–778. https://doi.org/10.5560/zna.2011-0042
[46] O.A. Hougen, K. M. Watson, R.A. Ragatz, Chemical Process Principles Charts, second ed., John Wiley & Sons, New York, 1960.
[47] L. Meng, Y.-Y. Duan, L. Li, Correlations for second and third virial coefficients of pure fluids, Fluid Phase Equilib. **226** (2004) 109–120. https://doi.org/10.1016/j.fluid.2004.09.023
[48] R.D. Mc Carty, Thermodynamic Properties of Helium 4 from 2 to 1500 K at Pressures of 10^8 Pa, J. Phys. Chem. Ref. Data **2** (1973) 923–1042. https://doi.org/10.1063/1.3253133

CRediT authorship contribution statement

Manuel Perez-Molina: Investigation; Methodology; Software; Writing–review & editing
M. F. Perez-Polo: Conceptualization; Formal analysis; Investigation; Methodology
F. J. Gil-Chica: Methodology; Supervision; Validation; Visualization
E. Fernández-Varó: Investigation; Methodology; Software; Writing–review & editing

Declaration of Competing Interest

The authors declare that they have no known competing financial interests or personal relationships that could have appeared to influence the work reported in this paper.